Virtual storage plants in parking lots of electric vehicles providing local/global power system support

Golmohammadi, Hessam

Published in:
Journal of Energy Storage

DOI (link to publication from Publisher):
10.1016/j.est.2021.103249

Publication date:
2021

Document Version
Publisher's PDF, also known as Version of record

Journal of Energy Storage 43 (2021) 103249

Contents lists available at ScienceDirect

Journal of Energy Storage

journal homepage: www.elsevier.com/locate/est

Virtual storage plants in parking lots of electric vehicles providing local/global power system support

Hessam Golmohamadi

Department of Computer Science, Aalborg University, Aalborg 9220, Denmark

ARTICLE INFO

Keywords:
Electric vehicle
Local/global service provider
Parking lot aggregator
Stochastic
Virtual storage plant

ABSTRACT

In recent years, the penetration of Renewable energy sources (RES) has increased considerably in power systems. Besides, fossil fuel vehicles are gradually replaced with electric ones. Increasing the penetration of RES on the supply side and the penetration of Plug-in electric vehicles (PEVs) on the demand side, intermittency of the power system increases. This paper proposes a novel structure for Virtual storage plants (VSP) to integrate the storage potentials of the PEVs into power systems. The suggested VSP is comprised of smart charging stations, Parking lot aggregator (PLA), Local service provider (LSP), and Global service provider (GSP). The PLA coordinates the charging/discharging strategies of the PEVs based on the flexibility requirements of the supply side. The LSP aims to mitigate congestion in weak lines of the power network. The GSP provides up-/down-regulation for the wholesale electricity market when a power shortage/excess occurs in the power systems. On the supply side, the electricity market is comprised of three trading floors, including the day-ahead, intraday, and balancing markets. The VSP integrates the storage potentials of the PEVs to the three market floors hierarchically on long, mid, and short advance notices. The electricity price data are extracted from the Danish electricity market. The suggested approach is examined on the IEEE 14-bus system. The results show that the suggested VSP provides local and global energy security for the power system during critical hours.

1. Introduction

1.1. Problem description and motivation

In Denmark, the penetration of Renewable energy sources (RES) was around 55% in 2020 and is scheduled to become 100% carbon-free by 2050 [1]. Besides, the Danish council on climate change suggests that the number of Plug-in electric vehicles (PEVs) should increase to 1 million by 2030 to achieve Denmark's goal of cutting emissions by 70% and becoming climate neutral no later than 2050. Increasing the penetration of RESs and PEVs concurrently, the intermittency and volatility of the power system increase considerably. To hedge against the uncertainties associated with RES and PEVs, Virtual power plant (VPP) and Virtual storage plant (VSP) are workable solutions. The VPP and VSP coordinate the Distributed generation (DG), energy storage, and flexible demands. The VPP/VSP concept has attracted much attention in recent years. Frequency and voltage regulations are key issues raised in VPP [2]. Besides, the VPP benefits from distributed energy storage systems to maintain power system stability [3]. The VPP is addressed as a prosumer not only to supply the domestic demand but also to provide power flexibility for the main grid through market bidding strategies [4]. PEVs are one of the most critical demands in VPP and VSP [5]. The main reason is that PEVs are mobile energy storage not only to provide global power system support [6], e.g. frequency control, but also to provide local distribution grid support, e.g. power congestion mitigation, through discharging to different charging stations in the network topology [7]. The energy storage capacity of PEVs can be extracted from private parking lots, i.e. residential parking [8], and public parking lots, e.g. airports [9], and shopping centers [10]. Regarding the recent advances in the energy storage capacity of PEVs, the main motivation of the current study is to characterize the public parking lots as a VSP providing local and global power system supports.

1.2. Literature review

In the traditional power systems, the large-scale centralized power plants were the main sources of electrical power. Recently, the penetration of Distributed energy resources (DER) has increased significantly in power systems worldwide. The DERs are small-scale energy resources including Distributed generator (DG), Energy storage system (ESS), and responsive (flexible) demands [11]. In this way, the VPP is cloud-based

E-mail address: hessamgolmoh@cs.aau.dk.

https://doi.org/10.1016/j.est.2021.103249
Received 29 April 2021; Received in revised form 3 September 2021; Accepted 21 September 2021
Available online 29 September 2021

Nomenclature

Acronyms

ADRA	agricultural demand response aggregator
CDRA	commercial demand response aggregator
CHP	combined heat and power
DER	distributed energy resource
DG	distributed generation
DoD	depth of discharge
DR	demand response
ESS	energy storage systems
GGDF	generalized generation distribution factors
GLDF	generalized load distribution factors
GSDF	generation shift distribution factors
GSP	global service provider
IDRA	industrial demand response aggregator
LSP	local service provider
PEV	plug-in electric vehicle
PDF	probability distribution function
PLA	parking lot aggregator
RDRA	residential demand response aggregator
RES	renewable energy sources
RPV	roof-top photovoltaic
SoC	state of charge
VPP	virtual power plant
VSP	virtual storage plant

Indices and sets

i	index of PEVs, $i = 1,\ldots,I$
j	index of PEV clusters, $j = 1,\ldots,J$
t	index of time, $t = 1,\ldots,T$
z	index of power system buses, $z = 1,\ldots,Z$
ω	index of electricity price scenarios, $\omega = 1,\ldots,\Omega$

Parameters and constants

$A_{l-k,z}$	GSDF of line between buses l and k due to change in power of bus z
$C_{l-k,z}$	GLDF of line between buses l and k due to power consumption in bus z
$D_{l-k,z}$	GGDF of line between buses l and k due to power generation in bus z
F_{l-k}^{max}	upper threshold of power flow for line between buses l and k (kW)
$SoC_{Arrive}^{i,j}$	SoC of PEV i from cluster j at arrival time
$SoC_{Departure}^{i,j,max}$	upper bound of SoC of PEV i from cluster j at departure time
$SoC_{Departure}^{i,j,min}$	lower bound of SoC of PEV i from cluster j at departure time
$SoC_{max}^{i,j}$	upper bound of SoC for PEV i from cluster j
$SoC_{min}^{i,j}$	lower bound of SoC for PEV i from cluster j
$t_{Arrival}^{i,j}$	arrival time of PEV i from cluster j
$t_{Arrival}^{i}$	arrival time of PEV i
$t_{Dwell}^{i,j}$	dwell time of PEV i from cluster j
t_{Dwell}^{i}	dwell time of PEV i
$\gamma_C^{i,j,max}$	upper bound for the charging rate of PEV i from cluster j
$\gamma_D^{i,j,max}$	upper bound for the discharging rate of PEV i from cluster j
$\eta_C^{i,j}$	charging efficiency of PEV i from cluster j
$\eta_D^{i,j}$	discharging efficiency of PEV i from cluster j
$\kappa^{i,j}$	presence state of PEV i from cluster j in the parking lot, 1 for presence and 0 for absence
κ^{max}	total space capacity of parking lot
$\lambda^{BM(-)}$	electricity price of balancing market during negative imbalance ($/kWh)
$\lambda^{BM(+)}$	electricity price of balancing market during positive imbalance ($/kWh)
λ^{DA}	electricity price of day-ahead market ($/kWh)
λ^{IM}	electricity price of intraday market ($/kWh)
κ(t)	total number of PEVs in parking lot at time slot t

Variables and functions

$\Delta\Pi_{C,z}^{PLA}$	incremental charging power of PLA connected to bus z (kW)
$\Delta\Pi_{D,z}^{PLA}$	incremental discharging power of PLA connected to bus z (kW)
$\Delta\Pi_{Net,z}^{PLA}$	incremental net power of PLA connected to bus z (kW)
ΔF_{l-k}	change in the power flow of line connected to buses l and k (kW)
$\Pi_{BM(-)}^{PLA}$	sold power to balancing market by PLA (kW)
$\Pi_{BM(+)}^{PLA}$	purchased power from balancing market by PLA (kW)
$\Pi_C^{i,j}(t)$	charging power of PEV i from cluster j at hour t (kW)
$\Pi_{DA,P}^{PLA}$	power purchased from day-ahead market by PLA (kW)
Π_{DA}^{PLA}	net power traded in day-ahead market by PLA (kW)
$\Pi_D^{(i,j)}(t)$	discharging power of PEV i from cluster j at hour t (kW)
$\Pi_{IM,P}^{PLA}$	power purchased from intraday market by PLA (kW)
$\Pi_{IM,S}^{PLA}$	power sold to intraday market by PLA (kW)
$\Pi_{Net}^{(i,j)}(t)$	net trading power of PEV i from cluster j at hour t (kW)
F_{l-k}	power flow of line between buses l and k
$F_{l-k}^{Congestion}$	the power flow of line between buses l and k at congestion mode
P_{l-k}	probability of congestion occurrence for line between buses l and k
P_z^G	active power generation at bus z (kW)
P_z^L	demand level at bus z (kW)
Q_z^G	reactive power generation at bus z (kVA)
$SoC_{Departure}^{i,j}(t)$	SoC of PEV i from cluster j at departure time t
$SoC^{(i,j)}(t)$	SoC of PEV i from cluster j at hour t
V_z	voltage magnitude at bus z (kV)
$\gamma_C^{(i,j)}(t)$	charging rate of PEV i from cluster j at hour t
$\gamma_D^{(i,j)}(t)$	discharging rate of PEV i from cluster j at hour t
δ_z	voltage angle at bus z
$\omega_C^{(i,j)}(t)$	binary variable of charging state, 1 for charging and 0 otherwise
$\varpi_D^{(i,j)}(t)$	binary variable of discharging state, 1 for discharging and 0 otherwise

management of DERs to coordinate the power generation capacities for the purpose of energy security and network efficiency [12].

The DGs normally refer to distributed wind turbines, Roof-top photovoltaic panels (RPV), Combined heat and power (CHP), and gas/diesel engines. Microwind turbines, in the forms of the vertical and horizontal axis, are broadly used in urban and remote areas to supply household energy consumption and battery charging [13]. The RPVs are small-scale photovoltaic panels that are installed on the rooftop of buildings. A significant number of RPVs in a city provides a considerable energy supply for the power system during high solar irradiation hours

[14]. The CHP makes it possible to provide heat and power for the district heating and power grid, respectively. The diesel engines are normally used for emergency backup of domestic power networks, e.g. residential buildings , commercial buildings, and farms.

Flexible demands are the part of electrical demands which can be changed/curtailed/shifted in response to an external request, e.g. Demand response (DR). The demand flexibility is defined for four demand sectors, including residential, e.g. heat pumps [15], industrial, e.g. cement manufacturing plants [16], agricultural, e.g. water irrigation pumps [17], and commercial sector, e.g. supermarket refrigerators. To coordinate flexibility potentials, Residential demand response aggregator (RDRA) [18], Industrial demand response aggregator (IDRA) [19], Agricultural demand response aggregator (ADRA) [20], and Commercial demand response aggregator (CDRA) [21] are suggested in the literature.

Energy storage is defined as the conversion of electrical energy from a power network into a form in which it can be stored until converted back to electrical energy [22]. The ESS normally stores energy during excess power generation (low price hours) to release during peak power demand (high price hours). Generally, the storage technologies can be classified into electrochemical, electromechanical, electromagnetic, and thermodynamic. Electrical batteries [23] and fuel cells [24] are key components of electrochemical storage. In electromagnetic storage, the electrical energy is stored in the form of a magnetic field, e.g. superconducting coils [25], or electric field, e.g. supercapacitors of PEVs [26]. Flywheels [27] and pumped hydro [28] are the most important applications of electromechanical storage. In thermodynamic energy storage, the energy is stored in the thermal dynamics of the storage medium like heat storage [29] and compressed air storage [30].

The VSP is comprised of the different types of ESS mentioned above (but not necessarily limited to). The VSP is responsible to coordinate the charging/discharging capacities of the ESS with the aim of energy security and power network efficiency. Although they are the general aims of the VSP, many research studies have been conducted in recent years to reduce operation cost [31], improve power system resilience [32], and enhance power system reliability [33]. Generally, the new-emerged entities, e.g. VPP, VSP, and DRA, aim to provide multiple network services. From the viewpoint of the power system, the support services are classified into two main categories as (1) local services (2) global services. The local services refer to the potentials to improve local power system variables, e.g. voltage profile and power congestion. The global services indicate the strategies that affect the global power system variables, e.g. power frequency, and power balance. In the former, the local transmission/distribution network takes advantage of the DERs. In the latter, the impacts of storage potentials are observed in the whole power system.

Regarding the local services, the key applications of the DERs can be surveyed as follows:

1, Voltage regulation (reactive power service) [34]
2. Power quality improvement [35]
3. Power congestion mitigation [36]
4. Power loss minimization [37]

In the case of global services, the following key objectives are pointed out:

1. Making power regulation (up/down) [38]
2. Providing frequency control [39]
3. Providing spinning reserve [40], non-spinning reserve [41], and supplemental reserve [42]
4. Facilitating the integration of RES into power systems [43]
5. Improving the power system reliability [44]
6. Reducing the investment cost [45]

In [45], the VSP is suggested to reduce network investment needs and to improve power system reliability at the distribution and transmission network levels. In [46], DERs are used to overcome under-voltage and over-voltage due to photovoltaic panels and PEVs, respectively. The study unlocks the flexibility potentials of responsive demands to regulate voltage profile in the distribution network in Japan. In [47], a coordination approach is suggested to improve power quality by using the aggregated ESS. The simulation results showed that the smart control of ESS could provide up to 60% peak-shaving in the distribution network of the UK. The Ref. [48] addresses the ESS as a practical tool to mitigate power congestion in both transmission and distribution lines. The simulation results show that the coordination scheme not only provides congestion relief but also facilitates RES integration. The paper [49] coordinates the operation of energy storage and photovoltaic panels to minimize the power loss in distribution lines as well as to improve the voltage profile in critical buses. The research study [50] proposes a multilevel approach to use the hybrid ESS, including ultracapacitors and lead-acid batteries, as the frequency support. The study suggests optimal control strategies to enable ultracapacitors and batteries to assist primary and secondary frequency responses, respectively. Paper [51] proposes a cooperative control framework of compressed air energy storage to provide frequency support for power systems. The results confirm that the approach confines the negative impacts of the demand and RES fluctuations on the power system frequency. In [52], multi-stage stochastic programming is addressed to use the flexibility potentials of distributed wind turbines and electrical batteries in providing power regulation for dynamic electricity markets. The suggested ESS charges/discharges the electrical power when a power excess/shortage occurs to provide down-/up-regulation for the electricity market. The paper [53] proposes a novel operational cost model for ESS, including Lithium-ion batteries, to provide energy and spinning reserve for electricity markets. The study concludes that the battery storage system improves the economic and technical operation of the power system by providing more options for system operation. The paper [54] proposes a self-scheduling approach for compressed air ESS that participates in energy, spinning, and non-spinning reserves markets.

Regarding PEVs, paper [55] proposes a distributed storage capacity formulation for commercial parking lots in the Istanbul metropolis. In [56], the car arrival/departure patterns are improved to extract practical storage capacity models for the parking lots of PEVs. Paper [57] suggests a stochastic framework for VPP to integrate flexibility potentials of EVs into uncertain electricity markets with high penetration of intermittent wind power. Finally, in [58], the storage potentials of EVs are investigated for two different parking lots, including shopping centers and workplaces. Moreover, the interactions between EV behaviors, e.g. arrival/departure times and charging/discharging patterns, and flexibility potentials are also studied.

To sum up, Fig. 1 depicts the schematic diagram of the VPP and VSP with the associated components.

1.3. Paper contributions and organization

Based on the review study, what is missing in the literature is to integrate the storage potentials of a significant number of PEVs providing local and global supports to power systems. To fulfill the aim, this study suggests a VSP, including smart charging stations, Parking lot aggregator (PLA), Local service provider (LSP), and Global service provider (GSP). The PLA coordinates the charging/discharging strategies of PEVs based on local and global flexibility requirements of the LSP and GSP, respectively. The LSP aims to mitigate congestion of transmission/distribution networks at critical hours. The GSP provides up-/down-power regulation during power system imbalances. Stochastic programming is addressed to optimize the operational strategies of the PLA under electricity price uncertainties. All in all, the main contributions of the study can be stated as follows:

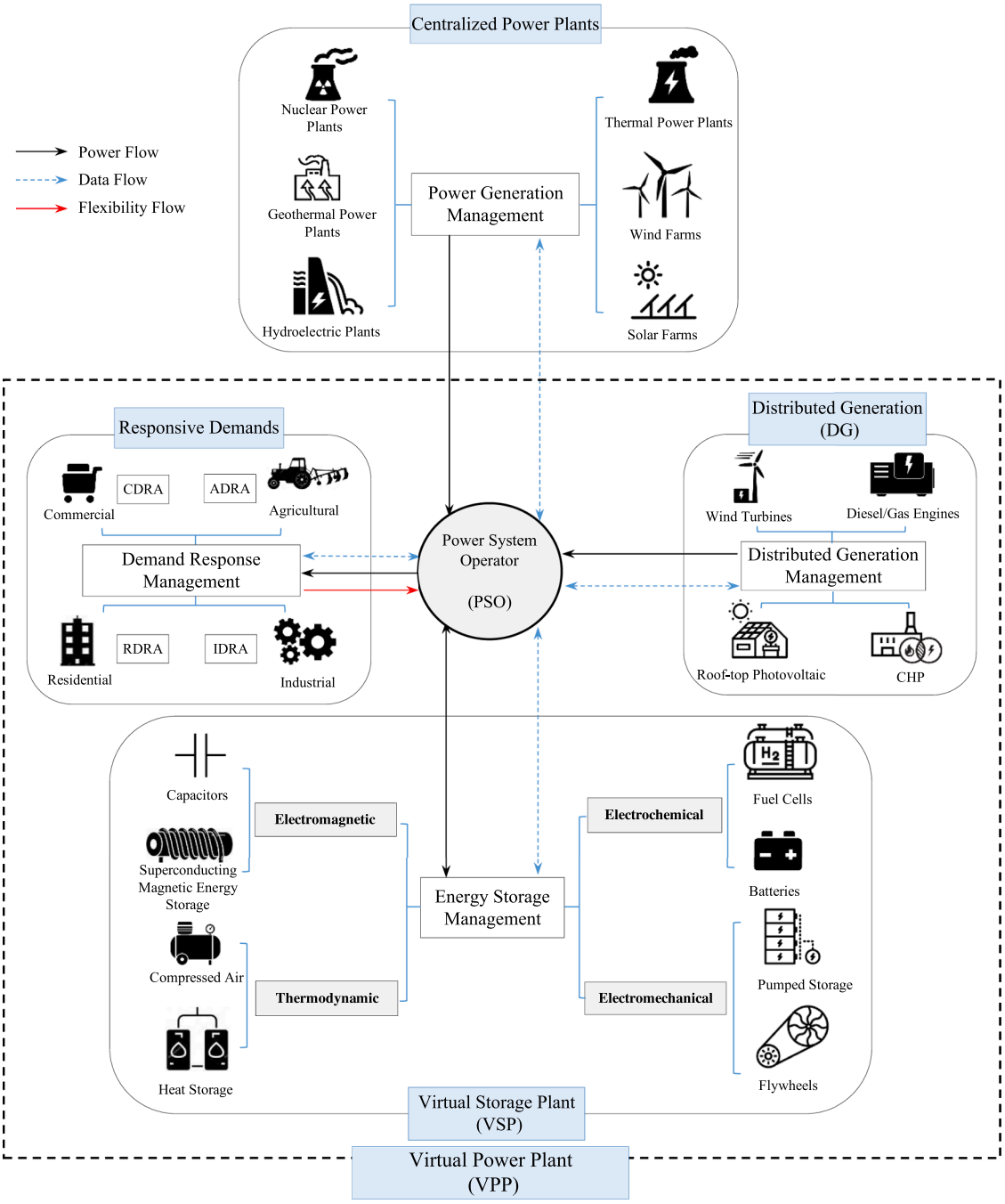

Fig. 1. Schematic diagram of the VPP and VSP in power systems.

1. Characterizing large-scale PLAs to unlock flexibility potentials of responsive PEVs.
2. Proposing a stochastic approach to provide up-/down-power regulation in uncertain electricity markets with high penetration of intermittent power.
3. Mitigating power congestion in local transmission/distribution grids through generalized distribution factor methods.

The rest of the paper is organized as follows. In Section 2, the fundamentals of the proposed approach are described qualitatively. In Section 3, the mathematical models of the VSP, including PEVs, PLA, LSP, and GSP, are explained. Section 4 is allocated to simulation results and discussions. Finally, Section 5 concludes the manuscript.

2. Problem description

This research study aims to integrate the storage potentials of a VSP into electricity markets with high RES penetration. On the demand side, the VSP is comprised of PLAs with smart charging stations. The PLAs manage large-scale parking lots with a significant number of PEVs. On the supply side, three trading floors of the Danish electricity market, including the day-ahead, intraday, and balancing markets, are addressed. The three market floors are cleared from 24 h before power delivery time until near real-time.

Fig. 2 describes the schematic structure of the parking lot as a VSP. As the figure reveals, the parking lots supply the parking spaces for different buildings, including office buildings, entertainment complexes, shopping centers, and food courts. Regarding the office buildings, the

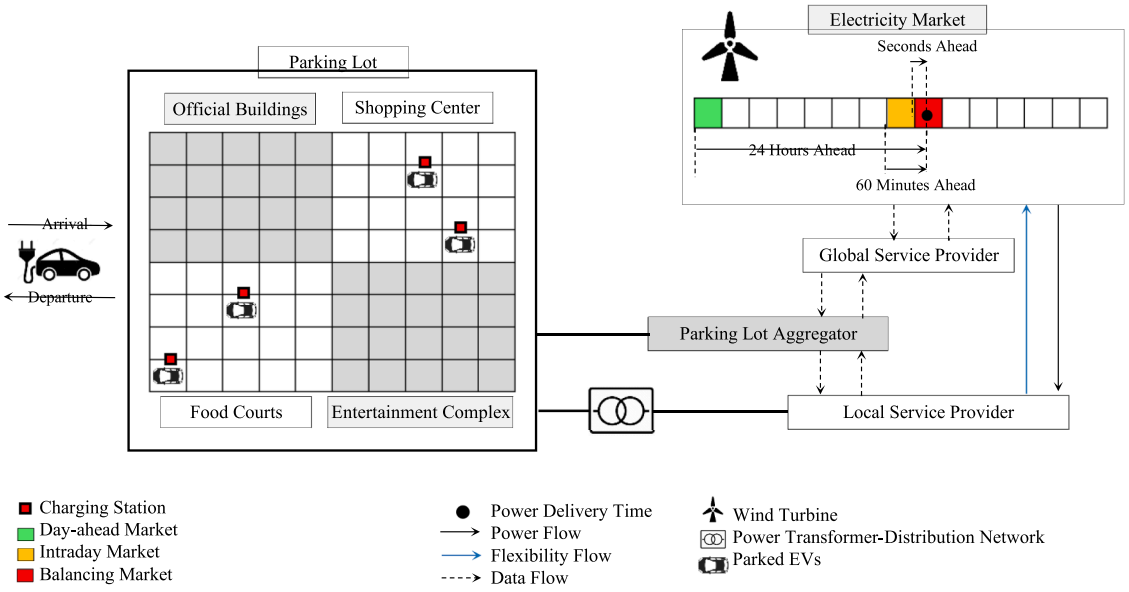

Fig. 2. The general structure of the parking lot as a VSP.

PEVs are parked normally from 8 am to 4 pm. Therefore, the office PEVs provide a considerable amount of storage capacity for around 8 h a day. Due to the long dwell time, this type of PEVs can provide demand flexibility for the day-ahead market on long advance notice. The rush time of entertainment complexes, e.g. cinema, and food courts, is normally from 6 pm to 10 pm. Moreover, the dwell time is less than the office PEVs, between 2 and 3 h. This feature makes them workable storage for flexibility requirements on mid advance notice in the intraday market. In the shopping center, the PEV owners spend normally around one hour shopping. This type of PEVs is a practical storage solution for balancing markets on short advance notice. The traffic data of the arking lots include the arrival time, arrival Stat of charge (SoC), preferred departure SoC, and departure time. To preprocess the raw traffic data, the PEVs are classified into different categories using the *k*-means clustering approach.

To coordinate the storage potentials of different PEVs, the smart charging stations are controlled by the PLA. The PLA receives the flexibility requirements from the GSP and LSP and offers price-based plans to motivate the PEV owners to participate in the DR programs.

The GSP integrates the storage potentials of the parking lots into electricity markets to provide global power regulation. When the electricity market faces a renewable power shortage, the PLA offers high electricity prices to the charging stations. The PEVs prefer to discharge to make a profit; as a result, the PEVs provide up-regulation for the power system. Adversely, when an excess renewable generation occurs, the PLA offers low electricity prices to charge the batteries. Consequently, the charging PEVs provide down-regulation for the power system. It is assumed that there is a strong correlation between RES availability and electricity price. Therefore, the electricity price conveys an important signal about RES availability. To cover the uncertainties associated with the electricity prices in the market floors, three-stage stochastic programming is addressed.

The LSP aims to use the storage potentials of the parking lots to mitigate local power congestion in weak grid lines. The contribution of each parking lot in congestion occurrence is calculated by using the distribution factors method. This method includes three types of factors, including Generation shift distribution factors (GSDF), Generalized generation distribution factors (GGDF), and Generalized load distribution factors (GLDF). These factors determine which parking lot at which bus has the highest impact on the congestion mitigation. As a result, the parking lot with the highest impact on the congestion is negotiated for power discharge to relieve the heavy congestion.

To make a comparison between Figs. 1 and 2, note that Fig. 1 sketches the general structure of VPP and VSP which is comprised of different DG, ESS, and flexible demands. Generally, a VSP/VPP may include some or all of the components. PEVs are one of the most important ESS which addresses electrical batteries. In this way, Fig. 2 describes the structure of the PLA as an intermediary agent to manage the storage potentials of PEVs. Therefore, Fig. 2 explains a specific VSP which emphasizes on storage potentials of electrical batteries of PEVs.

3. Problem formulation

In this section, the fundamentals of the suggested approach are modeled mathematically. For the sake of simplicity, the models are described in separate subsections.

3.1. Plug-in electric vehicle

In this study, the PEVs are the main source of energy storage. When the PEVs are parked in the parking lots, the PLA has access to a significant amount of electrical storage. The adequacy and availability of electrical storage are strongly dependent on the behavior of the PEV owners, e.g. arrival time, dwell time, arrival SoC, and preferred departure SoC. Therefore, the PEV owners' preferences should be addressed in the mathematical model. Without loss of generality, the mathematical model of PEVs can be stated as follows [59]:

$$\kappa(t) = \sum_{j=1}^{J} \sum_{i=1}^{I} \kappa^{i,j}(t) \tag{1}$$

$$0 \le \kappa(t) \le \kappa^{\max} \tag{2}$$

$$SoC^{i,j}_{Arrive}(t) = F_{Gaussian}\left(\mu, \sigma^2\right) \tag{3}$$

$$SoC^{i,j}(t) = SoC^{i,j}(t-1) + \left(\Pi^{i,j}_{C}(t) \times \eta^{i,j}_{C} \times \omega^{i,j}_{C}(t)\right) - \left(\frac{\Pi^{i,j}_{D}(t) \times \varpi^{i,j}_{D}(t)}{\eta^{i,j}_{D}}\right) \tag{4}$$

$$\gamma^{i,j}_{C}(t) = \frac{SoC^{i,j}(t) - SoC^{i,j}(t-1)}{\eta^{i,j}_{C}} \tag{5}$$

$$\gamma^{i,j}_{D}(t) = \left(SoC^{i,j}(t-1) - SoC^{i,j}(t)\right) \times \eta^{i,j}_{D} \tag{6}$$

$$0 \le \gamma_C^{i,j}(t) \le \gamma_C^{i,j,\max} \tag{7}$$

$$0 \le \gamma_D^{i,j}(t) \le \gamma_D^{i,j,\max} \tag{8}$$

$$SoC_{\min}^{i,j} \le SoC^{i,j}(t) \le SoC_{\max}^{i,j} \tag{9}$$

$$\Pi_{Net}^{i,j}(t) = \Pi_C^{i,j}(t) - \Pi_D^{i,j}(t) \tag{10}$$

$$SoC_{Departure}^{i,j,\min} \le SoC_{Departure}^{i,j}(t) \le SoC_{Departure}^{i,j,\max} \tag{11}$$

$$\omega_C^{i,j}(t) + \varpi_D^{i,j}(t) \le 1 \tag{12}$$

In this model, Eq. (1) describes the total number of PEVs present in the parking lots. The binary variable $\kappa^{i,j}$ shows the presence and absence of PEVs in which takes value 1 for the presence and 0 for the absence. Inequality (2) indicates the total capacity of the parking lots. Eq. (3) explains that the Gaussian probability distribution function (PDF) is used to estimate the SoC of PEVs at arrival time. Parameters μ and σ are the mean and standard deviation, respectively. In addition to Gaussian PDF, more PDFs, e.g. Normal and burr, are also stated in the literature. Eq. (4) explains the SoC of PEVs at time slot t as a function of previous SoC, charging, and discharging states. Eqs. (5) and (6) explain the rate of charging and discharging, respectively. The lower/upper bounds of charging and discharging rates are described by inequalities (7) and (8). Moreover, inequality (9) confines the SoC of PEVs to the lower and upper bounds. Eq. (10) shows the net power traded by the PEVs. Inequality (11) states the comfort bound of the PEV owners. The PEV owners are asked to set lower/upper thresholds for the preferred SoC at departure time. Finally, inequality (12) prevents concurrent charging and discharging states.

Fig. 3 describes the user interface panel of the charging stations. When a PEV is connected to the charging station, item 1, i.e. the arrival time, and item 2, i.e. the arrival SoC, are detected automatically by the charging station. The smart panel asks the PEV owner to input the estimated departure time and preferred SoC at departure time, including items 3 and 4, respectively. If the PEV owners are reluctant to participate in the charging/discharging strategies, items 3 and 4 must be left unfilled. The preferred lower and upper thresholds of SoC are addressed in the mathematical model by constraint (11).

3.2. Clustering of raw data

The commercial parking lots supply the buildings with different applications including office buildings, entertainment complexes, shopping centers, and food courts. The sociodemographic characteristics of the customers are various for different sections. For example, the customers of office buildings are employees who arrive normally at 8 am and leave the parking space around 4 pm. Therefore, this type of PEVs addresses a long dwell time with definite arrival and departure time. In contrast, the customers of shopping centers may dwell less time than the employees, around 1 and 2 h. Besides, the rush time of these customers normally occurs out of working hours. The sociodemographic features of the PEV owners are translated into the adequacy and availability of the electrical storage. As a result, the classification of PEVs with common features is a necessity for the PLA. The raw data of PEVs, including arrival time, arrival SoC, and dwell time, is classified into different clusters using *k*-means clustering. Each cluster has the most similar characteristics in terms of dwell time. The preprocessing of the raw data to obtain the clustered data can be stated as the following steps [60]:

Step 1. Collection of raw data: In the first step, the PLA collects the raw data required for the optimization of electrical storage. The input data includes the arrival time, arrival SoC, and dwell time. Therefore, the set of raw input data is stated as follows:

$$\forall i = 1, \ldots, I: \quad \mathrm{E}_{Raw} = \left\{ t_{Arrival}^{i}, SoC_{Arrival}^{i}, t_{Dwell}^{i} \right\} \tag{13}$$

Step 2. Clustering of raw data**:** In the second step, the set of input data $\mathrm{E_{Raw}}$ is classified into J clusters using *k*-means clustering while $J << I$. It means that the significant number of I initial PEVs are classified into J clusters. The members of cluster j∈J are selected in which each member (PEV) belongs to the cluster with the nearest centroid. The clustering criteria is the dwell time. Therefore, the members of each cluster have the most similarity in the case of dwell time. Consequently, the set of raw data is transformed into the clustered set as follows:

$$\left| \begin{matrix} \forall i = 1, \ldots, I \\ \forall j = 1, \ldots, J \end{matrix} \right| : \mathrm{E}_{Clustered} = \left\{ t_{Arrival}^{i,j}, SoC_{Arrival}^{i,j}, t_{Dwell}^{i,j} \right\} \tag{14}$$

Step 3. Data fitting**:** In the third step, the threshold SoC of PEVs at departure time are extracted from the best-fitted PDF. In this way, the Birnbaum-sanders, Gamma, Rayleigh, Log logistic, and Burr PDFs are addressed in the literature.

$$SoC_{Departure}^{i,j,\max/\min}(t) = \operatorname{argmax}[PDF_{Best-Fitted}] \tag{15}$$

As mentioned above, a significant number of PEVs is classified based on the dwell time. The main reason is that the length of dwell time determines the availability of the electrical storage for the supply side. The electricity market is comprised of three market floors including the day-ahead, intraday, and balancing markets. To integrate flexibility potentials of the electrical storage into the market floors, the PLA optimizes the charging/discharging strategies on long, mid, and short advance notices. Therefore, as the dwell time of the PEVs increases, the PEVs can participate in more market trading floors. This is the main idea behind clustering. To clarify the issue, Fig. 4 explains the classification of the PEVs into different clusters based on the dwell time.

3.3. Service providers

In this study, two types of service providers are considered including LSP and GSP. The LSP uses the storage potentials of the parking lots to mitigate congestion in weak lines of the local transmission/distribution networks. In contrast, the GSP provides up-/down-power regulation for the global electricity market in response to negative/positive power system imbalances.

3.3.1. Local service provider-LSP

In transmission/distribution networks, the local variables, e.g. power flow, may exceed the standard bound due to technical failure in the power facilities and/or peak consumption on the demand side. In such

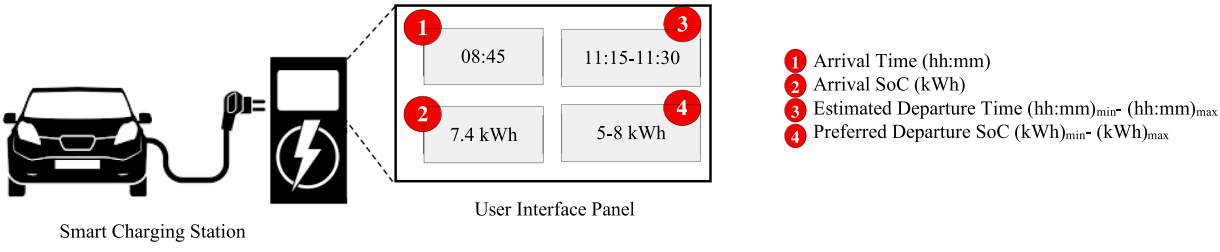

Fig. 3. User interface panel in the smart charging stations.

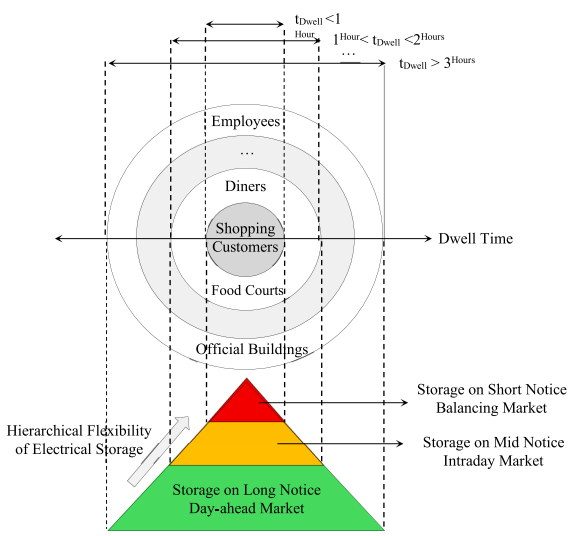

Fig. 4. Classification of PEVs into different clusters based on the dwell time.

conditions, the VSP integrates the flexibility potentials of the storage facilities to alleviate the heavy congestion in power lines. To fulfill the aim, the LSP is considered between the transmission/distribution network and the PLA. The LSP is an intermediary agent that receives the flexibility requirements from the power network to integrate the storage potentials of the PLAs. When heavy congestion occurs in the power network, the LSP asks the PLAs to discharge the parked PEVs. Therefore, the storage capacity supplies the local demands and alleviates the power congestion. To find out how the LSP translates the power congestion into charging/discharging strategies, the distribution factors method is adopted [61]. These factors determine the impact of PEVs' charging/-discharging on the power flow in grid lines. This method is stated as three factors including GSDF, GGDF, and GLDF.

- GSDF or *A* factors: The GSDF, or so-called *A* factors, determine line flow changes in the power lines due to a change in the power generation/consumption of buses. For a local power network with N_l lines and N_b buses, the *A* matrix with the dimension $N_l \times N_b$ is formed as $A = [a_{l\times b}]_{Nl\times Nb}$. Therefore, the array $a_{l\times b}$ shows the contribution of the generation/consumption of bus *b* in power flow of line *l*. GSDFs are calculated as follows:

$$\Delta F_{l-k} = A_{l-k,z} \times \Delta\Pi^{PLA}_{Net,z} \tag{16}$$

Eq. (16) describes the value of change in the power flow of the line between buses *l* and *k* when the PLA charges/discharges power from/to bus *z*. The GSDFs measure the incremental use of transmission and distribution networks in the charging and discharging modes of the storage units. The *A* factors are used to determine the share of charging/discharging batteries on the congestion variation in power lines. Note that the power variable $\Delta\Pi^{PLA}_{Net}$ refers to charging/discharging batteries when it takes positive/negative values.

- GLDF or *C* Factors: The GLDF, or *C* factors, determine the impact of the aggregated charging batteries on power flow in the transmission/distribution lines. The *A* factors determined the contribution of charging/discharging modes on the variation of power flow in distribution lines. Here, the *C* factors calculate the power flow in transmission lines using the value of charging/discharging power. Therefore, when congestion occurs in the power lines, the fast calculation of the power flow makes it possible to determine the best charging/discharging strategy to mitigate the congestion. The *C* factors are stated as follows [61]:

$$F_{l-k} = \sum_{z=1}^{Z} C_{l-k,z} \times \Delta\Pi^{PLA}_{C,z} \tag{17}$$

$$C_{l-k,z} = C_{l-k,r} - A_{l-k,z} \tag{18}$$

$$C_{l-k,r} = \left(F^{0}_{l-k} + \sum_{\substack{z=1 \\ z\neq r}}^{Z} \left(A_{l-k,z} \times \Pi^{PLA}_{C,z} \right) \right) \Big/ \sum_{z=1}^{Z} \Pi^{PLA}_{C,z} \tag{19}$$

Eqs (17)–(19) illustrates the variation in the power flow of the line between buses *l* and *k* when the PLA charges the batteries in bus *z*. Note that F^{0}_{l-k} denotes the power flow of line *l*-*k* before the congestion management.

- GGDF or *D* Factors: GGDF, or so-called *D* factors, determine the impact of the aggregated discharging batteries on power flow in the transmission/distribution lines. The *D* factors are calculated as follows [61]:

$$F_{l-k} = \sum_{z=1}^{Z} D_{l-k,z} \times \Delta\Pi^{PLA}_{D,z} \tag{20}$$

$$D_{l-k,z} = D_{l-k,r} + A_{l-k,z} \tag{21}$$

$$D_{l-k,r} = \left(F^{0}_{l-k} - \sum_{\substack{z=1 \\ z\neq r}}^{Z} \left(A_{l-k,z} \times \Pi^{PLA}_{D,z} \right) \right) \Big/ \sum_{z=1}^{Z} \Pi^{PLA}_{D,z} \tag{22}$$

Eqs. (20)–(22) explain how the power flow of the line between buses *l* and *k* changes when the PLA injects the discharging power to bus *z*.

By using factors, *A*, *C*, and *D*, the contribution of each PLA in the power congestion is determined. Let us consider a distribution network with *z* number of PLAs connected to z buses $z \in \{1,\ldots,Z\}$. When heavy congestion occurs in a power line, the LSP asks the PLAs to discharge the aggregated batteries to relieve the congestion. In this way, first of all, the LSP has to answer this question: "Which PLA is in top priority to discharge the batteries?". To find the best candidate, those PLAs should be selected whose discharging power has the highest impact on congestion mitigation. It means that the PLA with the biggest *A* factor is the highest priority. The LSP provides a priority list, also called a contingency list, that includes the PLAs with associated *A* factors in descending order. When congestion occurs in a power line, the contingency analysis shows which PLA has the most impact on the congestion relief. The LSP calculates the amount of discharging power for each PLA as follows:

$$\Delta\Pi^{PLA}_{D,z} = \frac{F^{Congestion}_{l-k} - F^{\max}_{l-k}}{A_{l-k,z}} \tag{23}$$

In power system operation, the power congestion occurs in the distribution network when the following probability is greater than a critical value:

$$P_{l-k} = \mathrm{Pro}b\left\{ F_{l-k} \geq F^{\max}_{l-k} \right\} \geq \sigma_{Critical} \tag{24}$$

If the probability (24) is satisfied, congestion management is a necessity. In this way, the LSP asks the candidate PLAs to discharge the

electrical storage into the distribution network. To mitigate congestion in weak lines, the power flow equations are run as follows:

$$f\left(P_z^G, Q_z^G, P_z^L, V_z, \delta_z\right) = 0 \tag{25}$$

$$P_z^{G,\min} \le P_z^G \le P_z^{G,\max} \tag{26}$$

$$Q_z^{G,\min} \le Q_z^G \le Q_z^{G,\max} \tag{27}$$

$$|F_{l-k}| \le F_{l-k}^{\max} \tag{28}$$

$$V_z^{\min} \le V_z \le V_z^{\max} \tag{29}$$

$$|\delta_z| \le \delta_z^{\max} \tag{30}$$

Eq. (25) denotes the set of power flow equations in power networks. Inequalities (26) and (27) describe the upper and lower thresholds of active and reactive power generation. The limitation of power flow in power lines is stated by (28). The inequalities (29) and ([29]) explain the limitation of voltage magnitude and angle, respectively.

To sum it up, when congestion occurs in the power lines, the LSP follows the following steps to relieve congestion:

Step 1: Provide the contingency list including *A* factors associated with each PLA $z = 1,\ldots, Z$.

Step 2: Sort the *A* factors in descending order.

Step 3: When congestion occurs, ask the PLA with the highest *A* factor to discharge power using Eq. (23).

Step 4: If the negotiated PLA provides the required discharging power, congestion alleviation is guaranteed. Otherwise, select the PLA with the next priority and go back to Step 3.

3.3.2. Global service provider-GSP

In contrast to the LSP, the GSP aims to provide global power regulation regardless of power network constraints. In this study, it is assumed that the VSP participates in the three trading floors of the electricity market, including the day-ahead, intraday, and balancing markets. The three market floors are adopted based on the Danish sector of the Nordic electricity market with 55% RES penetration [62]. In this electricity market, due to the intermittency of RES, the power management is firstly scheduled in the day-ahead market 24 h prior to energy delivery time; afterward, it is adjusted in the intraday market one hour ahead; and finally, it is regulated in the balancing market in near real-time. In this way, there is a strong correlation between the electricity price and RES availability. Besides, the electricity price is an uncertain variable due to imperfect data about renewable power generation. The PLA uses three-stage stochastic programming to optimize the charging/discharging strategies in the three market floors. The electricity prices of the three market floors are the main uncertain variables that are modeled by price scenarios. In the first stage of stochastic programming, the PLA participates in the day-ahead market 24 h before energy delivery time. In this stage, the day-head market is performed while the intraday and balancing markets are unclear. Therefore, the power procurement from the day-ahead market is a *here-and-now* variable and the power procurement from the intraday and balancing markets are *wait-and-see* variables. The objective function of the first stage can be stated as follows [59]:

$$\Psi^{FirstStage} = \underset{\left(\Pi_{DA}^{PLA}\right)}{Minimize}\left(\sum_{\omega=1}^{\Omega}\sum_{t=1}^{T} \mathrm{E}_{\omega_1}\left[\lambda^{DA}(t,\omega_1)\times\Pi_{DA}^{PLA}(t,\omega_1) + \Psi^{\mathrm{SecondStage}}\right]\right) \tag{31}$$

In the second stage, the PLA adjusts the charging/discharging strategies 60–10 min before energy delivery time. In this stage, the day-ahead market has already been cleared. The intraday market is performing while the balancing market is still unclear. Therefore, the power procurement from the intraday market is a *here-and-now* variable and the balancing power is *wait-and-see*. The objective function of the second stage is expressed as follows:

$$\Psi^{\mathrm{SecondStage}} = \underset{\left(\Pi_{IM}^{PLA}\right)}{Minimize}\left(\sum_{\omega=1}^{\Omega} \times \sum_{t=1}^{T} \mathrm{E}_{\omega_2\omega_1}\left[\lambda^{IM}(t,\omega_2)\times\Pi_{IM}^{PLA}(t,\omega_2) + \Psi^{ThirdStage}\right]\right) \tag{32}$$

In the third stage, the balancing market is run a few seconds before power delivery time. In this stage, the day-ahead and intraday markets have already been cleared. Therefore, the power procurement from the balancing market is *here-and-now*. While there is no pending market floor, no *wait-and-see* variable remains for further stages. The objective function of the third stage is formulated as follows:

$$\Psi^{ThirdStage} = \underset{\left(\Pi_{BM}^{PLA}\right)}{Minimize}\left(\sum_{\omega=1}^{\Omega}\sum_{t=\tau}^{T}\left[\mathrm{E}_{\omega_3\,\omega_1,\omega_2}\left[\left(\lambda^{BM(+)}(t,\omega_3)\times\Pi_{BM(+)}^{PLA}(t,\omega_3)\right) - \left(\lambda^{BM(-)}(t,\omega_3)\times\Pi_{BM(-)}^{PLA}(t,\omega_3)\right)\right]\right]\right) \tag{33}$$

As the objective function (33) reveals, the PLA uses two-price schemes for the balancing market, including positive and negative power system imbalances. In this market, when a power shortage occurs on the supply side, the power system imbalance is negative and the balancing electricity price increases considerably. Therefore, for the PLAs which provide up-regulation at the opposite side of the power system imbalance, the PEVs are paid by the balancing price more than the day-ahead price. In contrast, when excess power occurs on the supply side, the power system imbalance becomes positive and the balancing price decreases significantly. In such conditions, the GSP motivates the PLA to charge the PEVs by offering low electricity prices. Therefore, the PEVs are charged to provide down-regulation in the opposite direction of the power system imbalance. All in all, the two-price scheme can be formulated mathematically as follows:

$$\forall t \in \{1,\ldots,T\}: \begin{bmatrix} \left(\lambda_t^{BM(+)} \le \lambda_t^{DA}\right)^{Down-\mathrm{Regulation}} \\ \left(\lambda_t^{BM(-)} \ge \lambda_t^{DA}\right)^{Up-\mathrm{Regulation}} \end{bmatrix} \tag{34}$$

According to the two-price scheme, when a power shortage occurs, the PEVs that discharge to the power system are paid a high price. Adversely, the PEVs which are charged from the power grid have to pay a big price. In the hours with excess power, the PEVs pay low prices to charge. In contrast, the PEVs are paid a low price for discharging. This scheme encourages the PEVs to discharge/charge during power shortage/excess and discourages them to charge/discharge in the same direction of the power system imbalance.

The objective functions of the GSP are subjected to the following constraints:

$$\Pi_{DA}^{PLA}(t) = \Pi_{DA,P}^{PLA}(t) \tag{35}$$

$$\Pi_{IM}^{PLA}(t) = \Pi_{IM,P}^{PLA}(t) - \Pi_{IM,S}^{PLA}(t) \tag{36}$$

$$\Pi_{BM}^{PLA} = \Pi_{BM(+)}^{PLA} - \Pi_{BM(-)}^{PLA} \tag{37}$$

$$\Pi_{DA,P}^{PLA}(t) + \Pi_{IM,P}^{PLA}(t) + \Pi_{BM(+)}^{PLA} = \Pi_C^{PLA} \tag{38}$$

$$\Pi_{IM,S}^{PLA}(t) + \Pi_{BM(-)}^{PLA} = \Pi_D^{PLA} \tag{39}$$

$$\begin{vmatrix} \Pi_{BM(-)}^{PLA} \le \alpha \times \Pi_D^{PLA} \\ \Pi_{BM(+)}^{PLA} \le \alpha \times \Pi_C^{PLA} \end{vmatrix} \tag{40}$$

Eqs. (35)–(37) describe the net power traded in the three market floors as the summation of purchased and sold power with subscripts *P* and *S*, respectively. Note that the PLA only purchases power from the day-ahead market. Eqs. (38) and (39) show the power balance in the

charging and discharging modes. Inequality (40) confines the value of power trading in the balancing market to a fraction of charging/discharging power. The reason is that the balancing market is a volatile market with low power capacity to provide final up-/down-regulation. Therefore, a limited amount of power is traded. Also, this limitation may prevent power speculation by the PLAs.

All in all, the interactions between the LSP, GSP, and PLAs are illustrated in Fig. 5.

4. Numerical results and discussions

In this section, the case studies are described. The problem aims to provide local and global power system supports for the Danish electricity market for the next 24 h. To focus on the local and global system support, two case studies are examined as follows:

Case study 1: This case study aims to investigate the role of different PEV clusters in providing global power balance for the three market floors, i.e. the day-ahead, intraday, and balancing markets, through the GSP.

Case study 2: This case study aims to study the impact of different PLAs in providing local system support, i.e. congestion mitigation, in power lines through the LSP.

The mathematical models are coded in GAMS 24.1 [63], MATLAB 2019 [64], and MATPOWER 7.1 [65] and run by a laptop with an Intel CPU of 2 GHz and 16 GB of RAM.

4.1. Case study 1 of GSP

In this case, a large-scale public parking lot is simulated. The parking lot supplies four sections including office buildings, entertainment complexes, food courts, and shopping centers with parking capacities of 398, 252, 125, and 260 PEVs. Therefore, the total capacity of the PLA is 1035 vehicles. The input traffic data, including arrival time, dwell time, and maximum/minimum preferred departure SoC are synthesized using different PDFs. Fig. 6 sketches the arrival and departure of the office PEVs using Normal and Burr PDFs, respectively. As the bar graphs reveal, the arrival hour is between 7 and 9 and the departure time is concentrated on hours 15 and 16. Fig. 7 depicts the arrival and departure times for the entertainment complexes. In contrast to office PEVs with around 6–8 h of dwell time, the dwell time of the entertainment complexes is around 2–3 h.

Fig. 8 describes the arrival and departure times for the food courts. Based on the graphs, the rush times occur in two slots, including lunch and dinner. Besides, the dwell time is less than 2 h. Fig. 9 explains the traffic flow for the shopping center. The rush times occur in two durations, including morning and evening shopping. The dwell time is normally around 1 h.

In addition to the arrival and departure times, the arrival SoC and minimum/maximum preferred departure SoC are synthesized using PDFs. For the arrival SoC, Weibull PDF with scale parameter $\lambda_{wb} = 0.8$ and shape parameter $k_{wb} = 10$ is adopted. For the minimum and maximum departure SoC, the parameters of Weibull PDF are set to ($\lambda_{wb} = 0.4$, $k_{wb} = 10$) and ($\lambda_{wb} = 0.8$, $k_{wb} = 20$), respectively. Note that the capacity of electrical batteries is considered 50 kWh for all the clusters with the Depth of discharge (DoD) 10 kWh (20%).

Fig. 10 describes the electricity price uncertainties of the Danish electricity market for the next 24 h. Based on the graph, the day-ahead market faces two peak prices between hours 9–11 and 18–20. Similarly, the intraday market experiences a price jump in hours 11 and 18–20. In the balancing market, the significant increase of the electricity price in hours 8–10 is reflective of a renewable power shortage. In contrast, the near-zero electricity price in hours 12–17 shows an excess of renewable

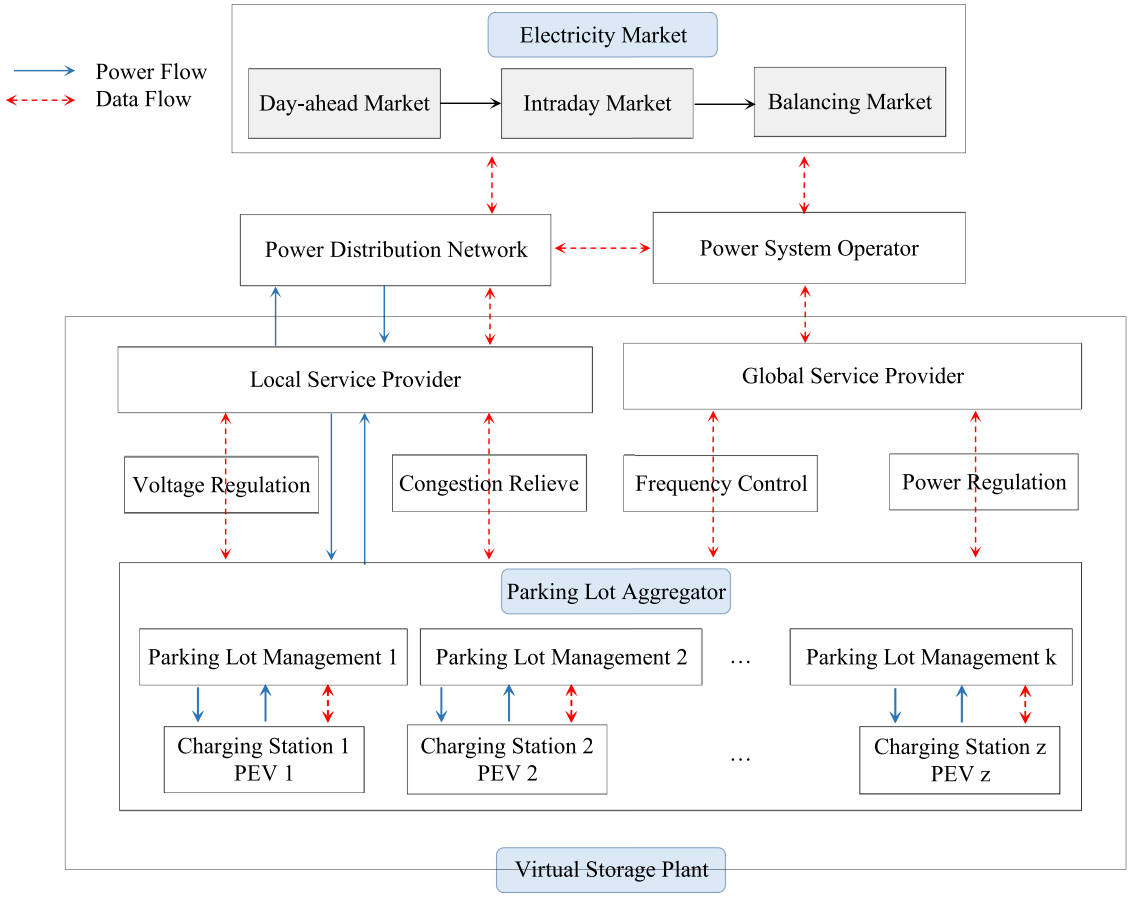

Fig. 5. Interactions between LSP, GSP, and PLAs in providing local and global power system support.

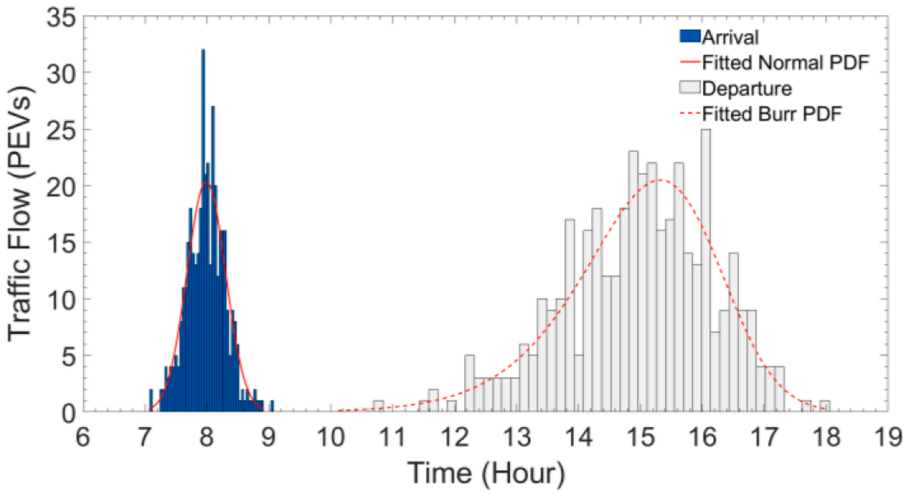

Fig. 6. Distribution of the arrival and departure for PEVs in the office buildings.

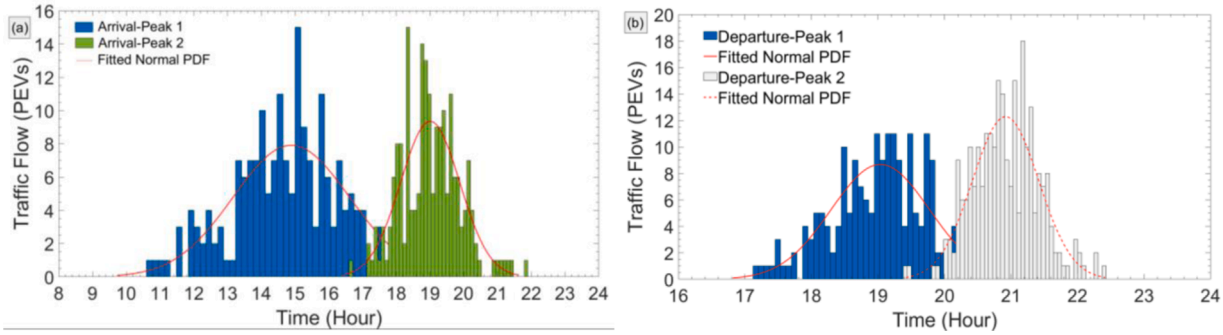

Fig. 7. Distribution of the arrival and departure for PEVs in the entertainment complexes (a) Arrival (b) Departure.

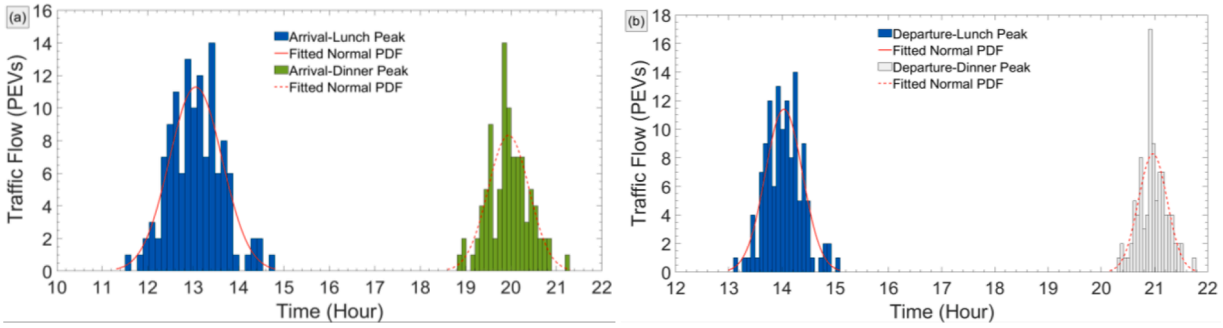

Fig. 8. Distribution of the arrival and departure for PEVs in the food court (a) Arrival (b) Departure.

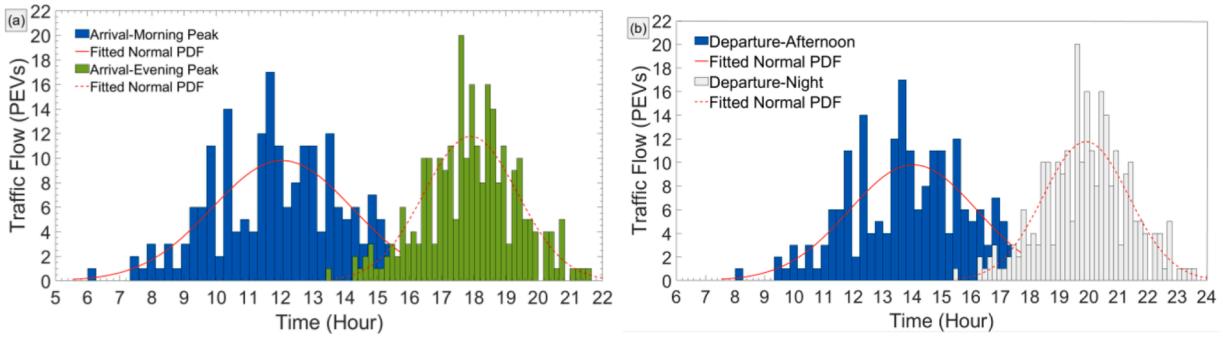

Fig. 9. Distribution of the arrival and departure for PEVs in the shopping center (a) Arrival (b) Departure.

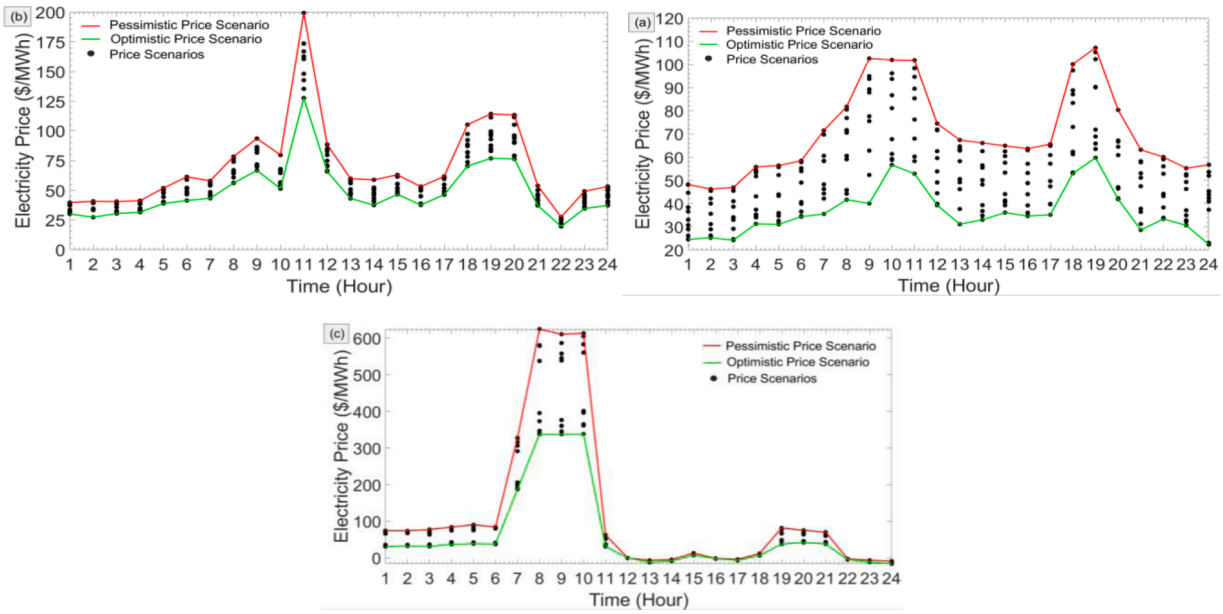

Fig. 10. Electricity market price scenarios for three market floors of Danish Electricity Market (a) Day-ahead (b) Intraday (c) Balancing market [66].

power.

Fig. 11 depicts the participation of four PEV clusters in the day-ahead market. In this figure, the expected value of day-ahead electricity price scenarios is depicted. As can be seen, the day-ahead market has two peak prices including 9–11 and 18–19, and two off-peak hours, including 12–17 and 20–24. Generally, all the PEVs prefer to charge in the off-peak hours when the electricity prices are relatively low. Adversely, the PEVs are reluctant to charge in peak price hours. Considering the office buildings, the PEVs provide storage flexibility in working hours, e.g. hours 11–12. The entertainment complex provides significant storage potential in hours 15–18 when the off-peak price hours coincide with the rush time of the PEVs. For the food courts, the PEVs provide flexibility potentials in lunchtime, hour 12, and dinner time 19–20, when the electricity prices are relatively low. The shopping center provides continuous low flexibility for the day-ahead market at most hours. The reason is that the dwell time of this cluster is low and vehicles arrival occurs gradually during the opening hours of the shopping center.

Fig. 12 explains the procurement strategies of the PLA in the intraday market. As the bar graph reveals, the general trend of the PEV clusters is to discharge power to the intraday market. In this way, barely charging power is seen except the morning hours 7–10. The reason is that the average electricity price of the intraday market is higher than the day-ahead market. Therefore, the PLA prefers to discharge the power storage to make a profit. Besides, the highest power discharge occurs at hour 11 when the intraday market experiences a huge increase in the electricity price. Assuming a renewable power shortage, the PEVs parked in the office sector inject a significant amount of power to adjust the power demand. The shopping center provides a continuous power discharge from hours 11 to 21. However, the value of power discharge is relatively lower than the other clusters. The main reason is that the dwell time of this cluster is low, around one hour; as a result, regardless of the significant number of PEV members, the PEVs are not deep discharged.

Fig. 13 describes the power trading strategies of the PLA in the balancing market. Regarding the profile of electricity price, the positive and negative power system imbalances are detected. Firstly, the balancing market faces an increase in the electricity price between hours 8 and 10. It shows that the balancing market faces a renewable power shortage, i.e. negative system imbalance. In contrast, the market encounters low electricity prices between hours 12–17 and 22–24. It means that an excess of renewable power shortage occurs; therefore, the power system faces a positive imbalance. In response to the negative system imbalances, the PLA discharges the PEVs of office buildings and shopping centers to provide up-regulation for the power system. In these hours, the PEVs of the other clusters are unavailable. When the positive

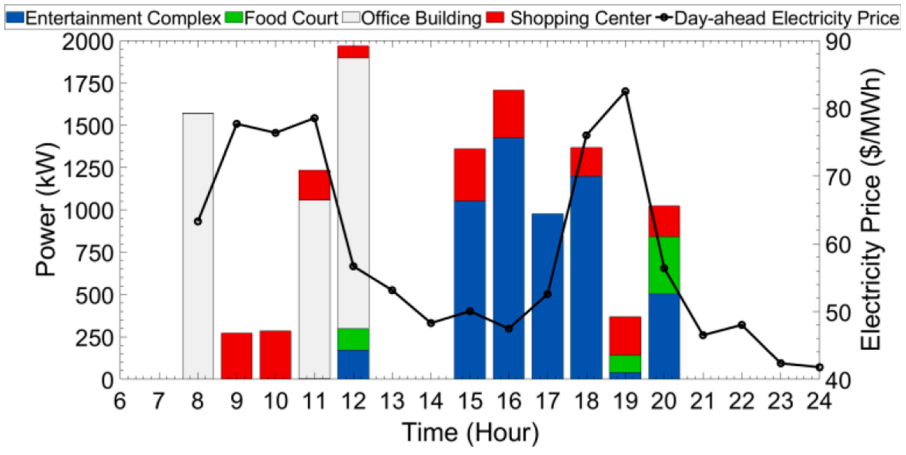

Fig. 11. Participation of PEV clusters in the day-ahead market.

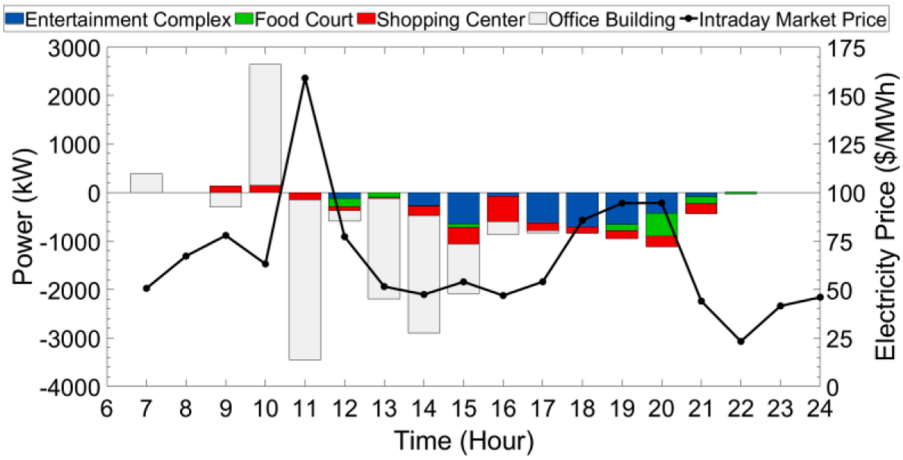

Fig. 12. Participation of PEV clusters in the intraday market.

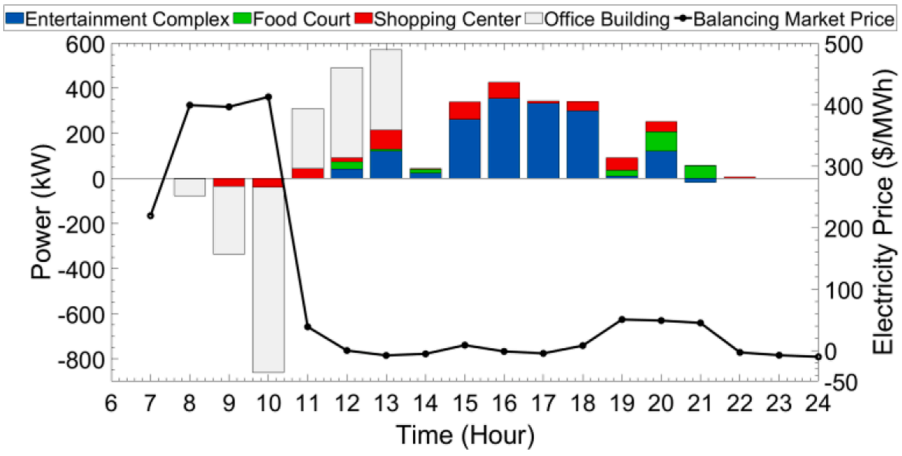

Fig. 13. Participation of PEV clusters in the balancing market.

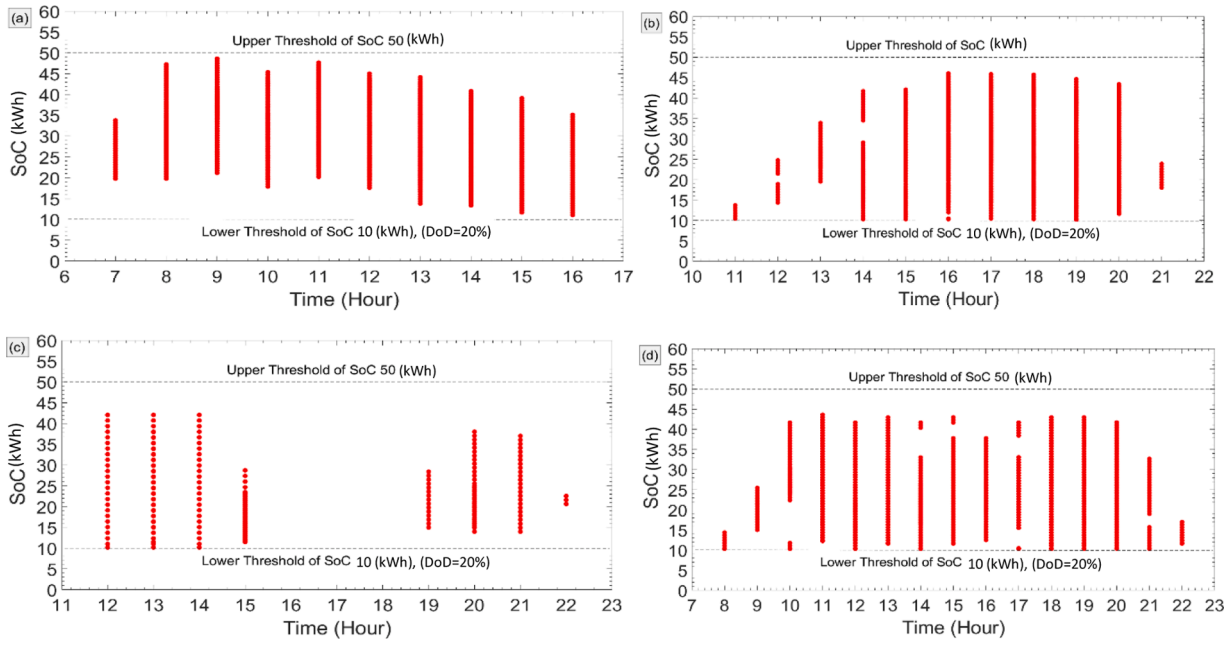

Fig. 14. SoC of PEVs in four clusters (a) Office buildings (b) Entertainment complex (c) Food court (d) Shopping center.

system imbalance occurs, all four clusters charge the batteries not only to provide down-regulation for the power system but also to take the advantage of low-price charging. Considering the participation of the PLA in the three market floors, it is shown that how the aggregation of a significant number of small-scale electrical batteries behaves as a VSP literally.

Fig. 14 depicts the SoC of the four clusters during the market operation. Based on the mathematical model, the upper and lower thresholds of the SoC are confined to maximum storage capacity and DoD of the batteries, respectively. Besides, the maximum/minimum preferred departure SoC of the PEV owners are set using the Weibull PDF. As the graphs reveal, the departure SoC of PEVs satisfies the owners' preferences.

In the primary case study, it is supposed that all the parking spaces are equipped with smart charging stations. In practical cases, the penetration of charging stations may be different. Therefore, a sensitivity analysis is conducted to study the impacts of the penetration of charging stations on the flexibility potentials of the parking lots. Table 1 illustrates the results. In this table, the net energy transactions in the three market floors are evaluated for four penetration factors, including 100, 75, 50, and 25%. Based on the results, as the penetration of charging stations decreases, the storage contribution of the parking lots decreases significantly. In addition, to investigate the impacts of arrival/dwell time on the flexibility potentials of the parking lots, Table 2 performs a sensitivity analysis. In this table, some scenarios are provided for arrival and dwell times. As the data reveals, by decreasing the dwell time, the energy transaction of the parking lot decreases. In some cases, the storage potential reaches zero points when no PEV is available in the time horizon. To sum up, the storage contributions of parking lots are strongly dependent on the penetration of charging stations and the arrival/dwell time of PEVs.

4.2. Case study 2 of LSP

In this case study, three PLAs are connected to different buses of the transmission network. The case study aims to show the contribution of the PLAs to congestion mitigation in power lines. To examine the suggested approach, the IEEE 14-bus system is addressed with 20 branches, 14 buses, 11 loads, and 5 generators. Detailed information about generation, demand level, and branch data can be found in [67]. Fig. 15 sketches the structure of the IEEE 14-bus system. In the test system, three PLAs are connected to buses 10, 12, and 14. Moreover, it is assumed that a failure causes power congestion in lines connected between buses 6–12, 6–13, and 7–9. The congested lines are pointed out in the figure.

Table 1
The impacts of penetration of charging stations on the storage capacity of the PLA.

Clusters	Penetration of charging stations	Day-ahead market	Intraday market	Balancing market
		Net transaction (kWh)	Net transaction (kWh)	Net transaction (kWh)
Office building	100 %	4221.6	-6759.6	-181.9
	75 %	3410.8	-4901.7	-116.1
	50 %	2250.7	-3259.8	-83.8
	25 %	985.4	-1742.4	-44.9
Entertainment complex	100 %	5373.3	-3634.7	1555.4
	75 %	4130.4	-2641.5	1056.4
	50 %	2624.7	-1875.3	862.1
	25 %	1221.8	-803.8	312.4
Food court	100 %	567.7	-1113.8	221.7
	75 %	410.5	-784.8	196.6
	50 %	287.4	-593.1	100.2
	25 %	129.8	-223.2	65.6
Shopping center	100 %	1978.2	-1926.7	386.6
	75 %	1405.8	-1487.9	299.1
	50 %	1084.4	-902.9	143.2
	25 %	421.7	-521.6	93.8

Table 2
The impacts of arrival and dwell times on the storage capacity of the PLA.

Clusters	Intervals of arrival/ departure times	Day-ahead market	Intraday market	Balancing market
		Net transaction (kWh)	Net transaction (kWh)	Net transaction (kWh)
Office building	7–18	4221.6	-6759.6	-181.9
	9–15	2652.6	-6685.3	-105.4
	12–13	1597.2	-2323.4	755.2
Entertainment complex	11–22	5373.3	-3634.7	1555.4
	13–20	5202.7	-3471.2	1493.2
	16–17	2400.9	-626.2	689.8
Food court	11–22	567.7	-1113.8	221.7
	14–20	438.8	-812.1	138.4
	15–18	0	-110.4	0
Shopping center	7–23	1978.2	-1926.7	386.6
	11–19	1238.3	-1875.5	417.4
	14–17	592.7	-973.3	153.2

Fig. 16 describes the profile of available SoC and the number of parked PEVs in the three parking lots during the study horizon, 24 h. Besides, the upper and lower thresholds of the storage capacities are shown in shaded areas. Regarding the blue area, it is assumed that all the parked PEVs are completely charged to the upper threshold of storage capacity. In contrast, the green area reflects the available discharging capacity where all the PEVs are deep discharged to reach the lower threshold of storage capacity, i.e. the predefined DoD.

Table 3 describes the results of power flow in the test system before congestion mitigation. Based on the table, it is assumed that an unforeseen failure causes power flow limitations on branches 12, 13, and 15. Therefore, the maximum power flow capacities of the power lines are reduced to 5.70, 15.34, and 26.50 MW, respectively. Regarding the power flow of 7.79, 17.75, and 28.07, congestion mitigation of 2.09, 2.41, and 1.57 MW is necessary for branches 12, 13, and 15, respectively.

To find the best candidate PLAs to discharge power, Table 4 states the GSDFs for the whole test system. For example, the intersection of bus 10 and line 7–9 indicates the value of -0.408. This value conveys that if 1 MW power congestion occurs in line 7–9, PLA 10 must discharge $\frac{1^{MW}}{0.408} = 2.45$ MW power to relief the congestion. Therefore, the PLA with the highest GSDF is the top priority for power discharging. Based on this fact, to mitigate congestion on branch 6–12, the descending priority is for PLAs 12, 14, and 10 with GSDFs -0.577, -0.84, and -0.015, respectively. Similarly, for branch 6–13, the priority is set as PLAs 14, 12, and 10. For branch 7–9, the priority list is defined as PLAs 10, 14, and 12.

Table 5 illustrates the features of congestion management. The third column describes the candidate PLAs based on the priority list. The fifth column states the hour of the congestion occurrence. Therefore, the congestion occurs in hours 12, 18, and 15 for lines 7–9, 6–12, and 6–13, respectively. From Fig. 16, the maximum discharging capacities, i.e. column six, are defined using the green shaded area. The minimum discharging powers are calculated by the division of power congestion and GSDF. Finally, column eight shows the value of power discharge by related PLA to mitigate the congestion. Note that by comparing columns six and eight, the value of discharging power is less than the discharging capacity; therefore, the first member of the priority list can supply the required power discharge for congestion relief.

Table 6 shows the results of power flow after congestion management in hours 12, 15, and 18. As the table reveals, by discharging the storage capacities to buses 10, 12, and 14, the power flows of branches

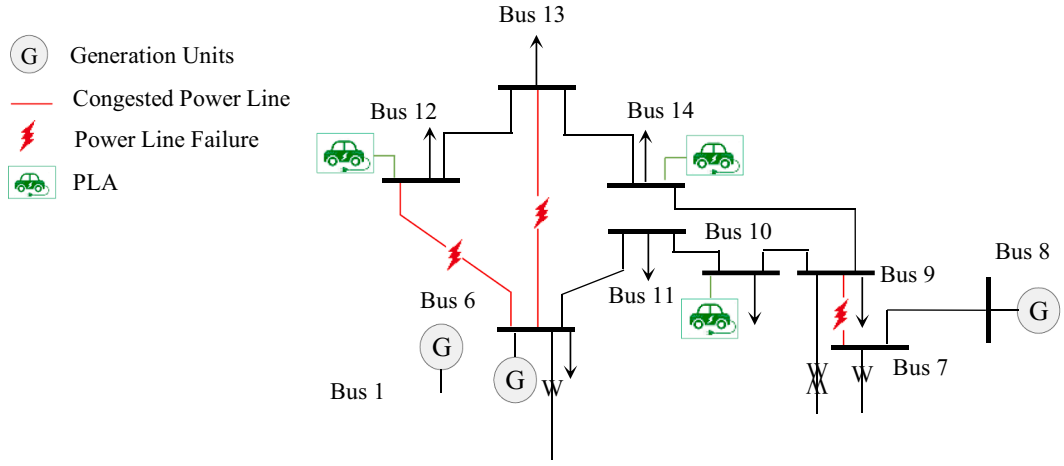

Fig. 15. Topology of the 14-bus IEEE-RTS with congested lines and connected PLAs.

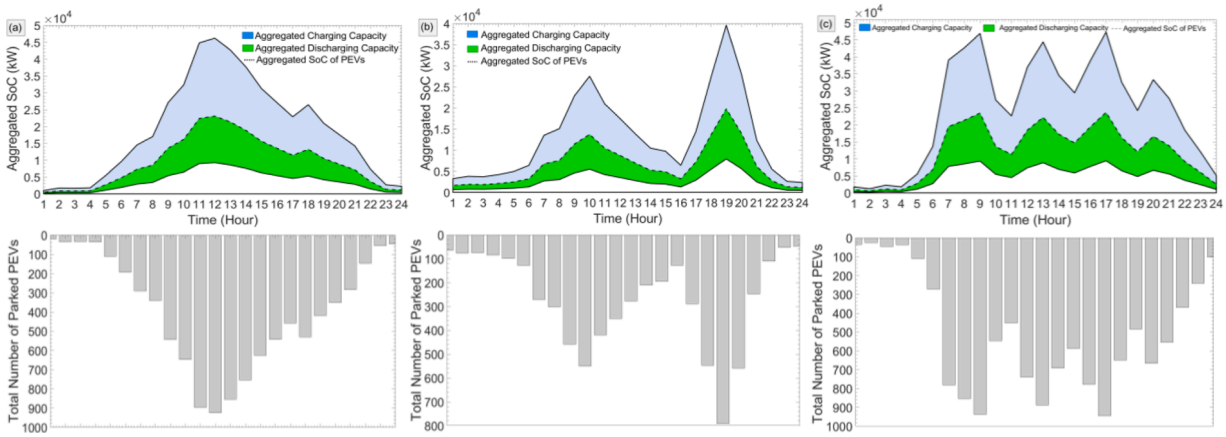

Fig. 16. Profile of SoC and PEV availability in the three parking lots (a) PLA of bus 10 (b) PLA of bus 12 (c) PLA of bus 14.

Table 3
Power flow in the IEEE 14-bus system with congested lines.

Branch No.	From bus	To bus	Active power (MW)	Max capacity of failed line (MW)	Congestion (MW)	Reactive power (MVAr)
1	1	2	156.88	-	-	-6.36
2	1	5	75.51	-	-	6.37
3	2	3	73.24	-	-	0.47
4	2	4	56.13	-	-	-0.48
5	2	5	41.52	-	-	1.59
6	3	4	-23.29	-	-	4.57
7	4	5	-61.16	-	-	11.58
8	4	7	28.07	-	-	-3.99
9	4	9	16.08	-	-	1.17
10	5	6	44.09	-	-	15.14
11	6	11	7.35	-	-	4.56
12	6	12	7.79	5.70	2.09	2.66
13	6	13	17.75	15.34	2.41	7.73
14	7	8	0.00	-	-	-8.05
15	7	9	28.07	26.50	1.57	3.01
16	9	10	5.23	-	-	3.20
17	9	14	9.43	-	-	2.95
18	10	11	-3.79	-	-	-2.64
19	12	13	1.61	-	-	0.91
20	13	14	5.64	-	-	2.42

15, 12, and 13 are back to the standard bound.

Fig. 17 describes the variation of aggregated SoC for three PLAs in response to congestion management. As can be seen, the SoC of the PLAs decreases to mitigate power congestion in lines 7–9, 6–12, and 6–13.

It is worth mentioning that the charging/discharging cycles increase battery degradation. The battery degradation cost affects the cost of energy storage in PEVs. Recently, the battery degradation cost model is developed to address the realistic battery performance degradation as much as possible during the charging and discharging processes [68]. Taking into account the wear price of electrical batteries, the charging/discharging strategies are reoptimized, especially when the PEVs are in the vehicle-to-grid state to provide power regulation, peak shaving, and enhancing power system reliability [69].

5. Conclusion

This paper proposed a novel structure to integrate the storage potentials of a significant number of PEVs into power systems. Mathematical models were suggested for a VSP which was comprised of PLAs, LSP, and GSP. The PLA was responsible for aggregating the storage potentials of parked PEVs. The LSP aimed to use the storage potentials of the PEVs to mitigate heavy congestion in weak lines during critical hours. To determine the contribution of PLAs in power congestion of the transmission network, the distributed factor method was addressed. The method enabled the LSP to set a priority list leveraging the most effective PLAs on the congested lines. Moreover, this made it possible to calculate the power flow in the congested lines without running the

Table 4
GSDFs (*A* Factors) for the 14 buses and 20 branches of the IEEE 14-bus system.

Line		Bus No.												
from	to	1	2	3	4	5	6	7	8	9	10	11	12	13	14
1	2	0	-0.858	-0.827	-0.725	-0.655	-0.675	-0.717	-0.717	-0.712	-0.709	-0.695	-0.687	-0.693	-0.718
1	5	0	-0.166	-0.276	-0.352	-0.404	-0.385	-0.361	-0.361	-0.365	-0.371	-0.379	-0.389	-0.390	-0.383
2	3	0	0.027	-0.570	-0.161	-0.109	-0.125	-0.154	-0.154	-0.150	-0.147	-0.136	-0.129	-0.131	-0.145
2	4	0	0.057	-0.142	-0.320	-0.218	-0.249	-0.303	-0.303	-0.293	-0.287	-0.269	-0.256	-0.260	-0.284
2	5	0	0.078	-0.068	-0.204	-0.293	-0.264	-0.220	-0.220	-0.229	-0.237	-0.251	-0.265	-0.264	-0.249
3	4	0	-0.027	-0.456	0.158	0.107	0.123	0.151	0.151	0.147	0.144	0.134	0.126	0.129	0.142
4	5	0	-0.078	-0.308	-0.497	0.307	0.058	-0.353	-0.353	-0.277	-0.218	-0.082	0.034	0.011	-0.153
4	7	0	0.003	0.013	0.023	-0.009	-0.196	-0.631	-0.631	-0.451	-0.408	-0.304	-0.217	-0.237	-0.364
4	9	0	0.002	0.008	0.014	-0.005	-0.112	-0.165	-0.165	-0.257	-0.232	-0.174	-0.124	-0.135	-0.207
5	6	0	-0.005	-0.021	-0.037	0.014	-0.687	-0.207	-0.207	-0.297	-0.368	-0.527	-0.668	-0.644	-0.459
6	11	0	-0.003	-0.013	-0.022	0.009	0.191	-0.125	-0.125	-0.179	-0.291	-0.544	0.167	0.140	-0.043
6	12	0	0.000	-0.002	-0.003	0.001	0.023	-0.016	-0.016	-0.023	-0.015	0.003	-0.577	-0.159	-0.084
6	13	0	-0.002	-0.006	-0.012	0.004	0.097	-0.064	-0.064	-0.092	-0.060	0.017	-0.252	-0.617	-0.327
7	8	0	0.000	0.000	0.000	0.000	0.000	0.000	1.000	0.000	0.000	0.000	0.000	0.000	0.000
7	9	0	0.003	0.013	0.023	-0.009	-0.196	0.369	0.369	-0.451	-0.408	-0.304	-0.217	-0.237	-0.364
9	10	0	0.003	0.013	0.022	-0.009	-0.189	0.124	0.124	0.178	-0.713	-0.457	-0.166	-0.138	0.042
9	14	0	0.002	0.008	0.014	-0.005	-0.118	0.079	0.079	0.113	0.073	-0.020	-0.174	-0.231	-0.607
10	11	0	-0.003	-0.013	-0.022	0.009	0.189	-0.124	-0.124	-0.178	-0.289	0.458	0.166	0.139	-0.042
12	13	0	0.000	-0.002	-0.003	0.001	0.023	-0.016	-0.016	-0.023	-0.015	0.003	0.426	-0.157	-0.083
13	14	0	-0.002	-0.008	-0.014	0.005	0.118	-0.079	-0.079	-0.113	-0.073	0.020	0.174	0.231	-0.403

Table 5
Technical characteristics of the congestion management.

Line		Candidate responsive PLA (Bus No.)	GSDF	Hour of Congestion Occurrence (h)	Maximum discharging Capacity (kW)	Minimum congestion (kW)	Minimum discharging Power (kW)
From	To						
7	9	10	-0.408	12	13860	1570	(1570/-0.408) = -3848
6	12	12	-0.577	18	8205	2090	(2090/-0.577) = -3622
6	13	14	-0.327	15	8820	2410	(2410/-0.327) = -7370

Table 6
Power flow of the test system after congestion management in hours 12, 15, and 18.

Power lines			Power flow at hour 12		Power flow at hour 18		Power flow at hour 15	
Branch	From bus	To bus	Active power (MW)	Reactive power (MVAr)	Active power (MW)	Reactive power (MVAr)	Active power (MW)	Reactive power (MVAr)
1	1	2	154.08	-19.75	154.33	-19.81	151.48	-19.13
2	1	5	74.03	3.67	74.05	3.70	72.59	3.51
3	2	3	72.66	3.62	72.76	3.61	72.14	3.67
4	2	4	54.99	-1.72	55.18	-1.61	53.98	-1.84
5	2	5	40.59	1.01	40.54	1.07	39.65	0.89
6	3	4	-23.83	4.26	-23.73	4.38	-24.31	4.11
7	4	5	-60.33	15.73	-61.28	15.57	-60.04	15.57
8	4	7	26.50	-9.71	27.29	-9.52	25.40	-9.66
9	4	9	15.18	-0.52	15.63	-0.34	14.56	-0.53
10	5	6	42.67	12.66	41.67	12.53	40.73	12.78
11	6	11	6.23	3.57	7.96	3.35	7.04	3.40
12	6	12	7.73	2.51	5.68	2.17	7.16	2.54
13	6	13	17.52	7.21	16.83	7.28	15.33	6.95
14	7	8	0.00	-16.78	0.00	-17.12	0.00	-16.55
15	7	9	26.50	5.53	27.29	5.99	25.40	5.47
16	9	10	2.48	4.15	4.63	4.45	5.54	4.37
17	9	14	9.71	3.60	8.79	3.79	4.92	3.48
18	10	11	-2.68	-1.67	-4.38	-1.38	-3.48	-1.47
19	12	13	1.56	0.76	3.16	0.48	1.00	0.81
20	13	14	5.36	1.76	6.28	1.56	2.66	1.64

power flow for the whole system. The GSP provided up-/down-regulation for the three market floors of the Danish electricity market with high penetration of RES when a power shortage/excess occurs. To hedge against the electricity price uncertainties, three-stage stochastic programming was formulated to schedule, adjust and finally regulate power charging/discharging on long, mid, and short advance notices.

The simulation results of the LSP showed that the distribution factor method provides a priority list to discharge the parking lots connected to different buses. The discharged power could mitigate the power congestion in weak lines effectively. The key point was that the method identified the buses with the highest impact on the congestion mitigation; therefore, the lowest power discharge was requested to relieve the congestion. The simulation results of the GSP confirmed that a significant number of PEVs can integrate storage potentials to the electricity market when the power system faces a deficit/excess of RES. The availability of storage potentials had a strong correlation with the sociodemographic characteristics of the PEV owners. In this way, the arrival and dwell times played key roles. For PEVs with long dwell time,

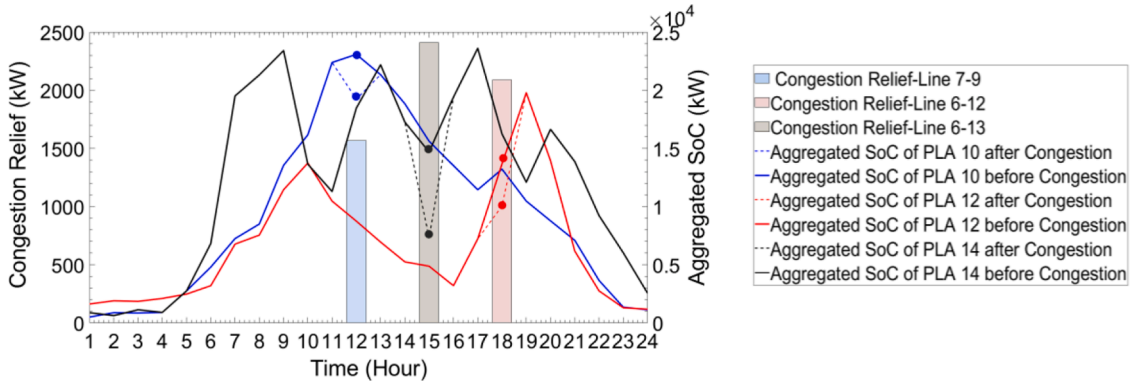

Fig. 17. Reduction in the aggregated SoC of PLAs in response to congestion mitigation.

e.g. office buildings, the PLA guaranteed a considerable amount of storage potential during working hours. In contrast, for the shopping centers with low dwell time, the PLA provided low values of the storage potential in the most hours a day. Besides, it was shown that the PEVs could participate actively in the balancing market not only to redress the negative/positive power system imbalances but also to charge/discharge batteries with low/high electricity prices.

Modeling the LSP and GSP, the study showed the role of VSP in providing local and global system support literally. Although the following suggestions may be the subject of further investigations by the enthusiastic researchers:

1. Regarding the LSP, the PLA participated in congestion management. The other local services, e.g. voltage compensation, enhancing resilience, are of interest in these studies.
2. In this study, it is assumed that all parked PEVs participate in the DR programs. The uncertainty of the PEV participation may affect the operation of the VSP.
3. In this approach, the arrival time of PEVs is modeled using the Weibull distribution function. One may examine the impacts of other probability distribution functions on power storage availability.
4. The battery degradation cost may affect the charging/discharging strategies of PEVs in power grid applications. One may integrate the degradation cost of PEV batteries into the charging/discharging scheduling.

Funding: The study is supported by the FEVER project (Flexible Energy Production, Demand and Storage-based Virtual Power Plants for Electricity Markets and Resilient DSO Operation), Department of Computer Science, Aalborg University, Denmark (European Union's Horizon 2020).

CRediT authorship contribution statement

Hessam Golmohamadi: Conceptualization, Methodology, Software, Data curation, Writing – original draft.

Declaration of Competing Interest

The authors declare that they have no known competing financial interests or personal relationships that could have appeared to influence the work reported in this paper.

References

[1] H. Golmohamadi, R. Keypour, B. Bak-Jensen, J.R. Pillai, Optimization of household energy consumption towards day-ahead retail electricity price in home energy management systems, Sustain. Cities Soc. 47 (2019), 101468, https://doi.org/10.1016/j.scs.2019.101468.
[2] R. Zhang, B. Hredzak, Distributed dynamic clustering algorithm for formation of heterogeneous virtual power plants based on power requirements, IEEE Trans. Smart Grid 12 (1) (2021) 192–204, https://doi.org/10.1109/TSG.2020.3020163.
[3] N. Zhi, K. Ding, L. Du, H. Zhang, An SOC-based virtual DC machine control for distributed storage systems in DC microgrids, IEEE Trans. Energy Convers. 35 (3) (2020) 1411–1420, https://doi.org/10.1109/TEC.2020.2975033.
[4] W. Tang, H. Yang, Optimal operation and bidding strategy of a virtual power plant integrated with energy storage systems and elasticity demand response, IEEE Access 7 (2019) 79798–79809, https://doi.org/10.1109/ACCESS.2019.2922700.
[5] B. Zhou, et al., Optimal coordination of electric vehicles for virtual power plants with dynamic communication spectrum allocation, IEEE Trans. Ind. Inform. 17 (1) (2021) 450–462, https://doi.org/10.1109/TII.2020.2986883.
[6] W. Wang, P. Chen, D. Zeng, J. Liu, Electric vehicle fleet integration in a virtual power plant with large-scale wind power, IEEE Trans. Ind. Appl. 56 (5) (2020) 5924–5931, https://doi.org/10.1109/TIA.2020.2993529.
[7] M.T. Kahlen, W. Ketter, J. van Dalen, Electric vehicle virtual power plant dilemma: grid balancing versus customer mobility, Prod. Oper. Manag. 27 (11) (2018) 2054–2070, https://doi.org/10.1111/poms.12876. Nov.
[8] M. Mozaffari, H.A. Abyaneh, M. Jooshaki, M. Moeini-Aghtaie, Joint expansion planning studies of EV parking lots placement and distribution network, IEEE Trans. Ind. Inform. 16 (10) (2020) 6455–6465, https://doi.org/10.1109/TII.2020.2964049.
[9] M. Maigha, M.L. Crow, A transactive operating model for smart airport parking lots, IEEE Power Energy Technol. Syst. J. 5 (4) (2018) 157–166, https://doi.org/10.1109/JPETS.2018.2876453.
[10] U.B. Irshad, M.S.H. Nizami, S. Rafique, M.J. Hossain, S.C. Mukhopadhyay, A battery energy storage sizing method for parking lot equipped with EV chargers, IEEE Syst. J. (2020) 1–11, https://doi.org/10.1109/JSYST.2020.3009695.
[11] K. Mahmud, B. Khan, J. Ravishankar, A. Ahmadi, P. Siano, An internet of energy framework with distributed energy resources, prosumers and small-scale virtual power plants: an overview, Renew. Sustain. Energy Rev. 127 (2020), 109840, https://doi.org/10.1016/j.rser.2020.109840.
[12] S.M. Nosratabadi, R.A. Hooshmand, E. Gholipour, A comprehensive review on microgrid and virtual power plant concepts employed for distributed energy resources scheduling in power systems, Renew. Sustain. Energy Rev. 67 (2017) 341–363, https://doi.org/10.1016/j.rser.2016.09.025.
[13] D.X. Llano, R.A. McMahon, Control techniques with system efficiency comparison for microwind turbines, IEEE Trans. Sustain. Energy 8 (4) (2017) 1609–1617, https://doi.org/10.1109/TSTE.2017.2698024.
[14] H. Golmohamadi, R. Keypour, A bi-level robust optimization model to determine retail electricity price in presence of a significant number of invisible solar sites, Sustain. Energy Grids Netw. 13 (2018) 93–111, https://doi.org/10.1016/j.segan.2017.12.008.
[15] H. Golmohamadi, K. Guldstrand Larsen, P. Gjøl Jensen, I. Riaz Hasrat, Optimization of power-to-heat flexibility for residential buildings in response to day-ahead electricity price, Energy Build. 232 (2021), 110665, https://doi.org/10.1016/j.enbuild.2020.110665.
[16] H. Golmohamadi, A. Asadi, Integration of joint power-heat flexibility of oil refinery industries to uncertain energy markets, Energies 13 (18) (2020), https://doi.org/10.3390/en13184874.
[17] H. Golmohamadi, A. Asadi, A multi-stage stochastic energy management of responsive irrigation pumps in dynamic electricity markets, Appl. Energy 265 (2020), 114804, https://doi.org/10.1016/j.apenergy.2020.114804.
[18] H. Golmohamadi, R. Keypour, B. Bak-Jensen, J.R. Pillai, A multi-agent based optimization of residential and industrial demand response aggregators, Int. J. Electr. Power Energy Syst. 107 (2019) 472–485, https://doi.org/10.1016/j.ijepes.2018.12.020.
[19] H. Golmohamadi, R. Keypour, B. Bak-Jensen, J.R. Pillai, M.H. Khooban, Robust self-scheduling of operational processes for industrial demand response aggregators, IEEE Trans. Ind. Electron. 67 (2) (2020) 1387–1395, https://doi.org/10.1109/TIE.2019.2899562. Feb.
[20] H. Golmohamadi, Operational scheduling of responsive prosumer farms for day-ahead peak shaving by agricultural demand response aggregators, Int. J. Energy Res. (2021), https://doi.org/10.1002/er.6017 n/a, no. n/a.

[21] G. Lipari, G. Del Rosario, C. Corchero, F. Ponci, A. Monti, A real-time commercial aggregator for distributed energy resources flexibility management, Sustain. Energy, Grids Netw. 15 (2018) 63–75, https://doi.org/10.1016/j.segan.2017.07.002.

[22] A. Price, 12 - Energy Storage for Small and Micro Combined Heat and Power (CHP) Systems, Woodhead Publishing, 2011, pp. 307–322. *Woodhead Publishing Series in Energy*, R. B. T.-S. and M. C. H. and P. (CHP) S. Beith, Ed.

[23] Y. Wang, X. Ai, Z. Tan, L. Yan, S. Liu, Interactive dispatch modes and bidding strategy of multiple virtual power plants based on demand response and game theory, IEEE Trans. Smart Grid 7 (1) (2016) 510–519, https://doi.org/10.1109/TSG.2015.2409121.

[24] H. Khasawneh, M. Illindala, Supercapacitor cycle life equalization in a microgrid through flexible distribution of energy and storage resources, IEEE Trans. Ind. Appl. 51 (3) (2015) 1962–1969, https://doi.org/10.1109/TIA.2014.2369815.

[25] M.G. Molina, P.E. Mercado, Power flow stabilization and control of microgrid with wind generation by superconducting magnetic energy storage, IEEE Trans. Power Electron. 26 (3) (2011) 910–922, https://doi.org/10.1109/TPEL.2010.2097609.

[26] Q. Zhang, W. Deng, G. Li, Stochastic control of predictive power management for battery/supercapacitor hybrid energy storage systems of electric vehicles, IEEE Trans. Ind. Inform. 14 (7) (2018) 3023–3030, https://doi.org/10.1109/TII.2017.2766095.

[27] S. Adhikari, R. Karki, Integrated disturbance response modeling of wind-integrated power systems to quantify the operational reliability benefits of flywheel energy storage, IEEE Trans. Sustain. Energy 10 (3) (2019) 1152–1160, https://doi.org/10.1109/TSTE.2018.2862351.

[28] N. Lou, et al., Two-stage congestion management considering virtual power plant with cascade hydro-photovoltaic-pumped storage hybrid generation, IEEE Access 8 (2020) 186335–186347, https://doi.org/10.1109/ACCESS.2020.3030637.

[29] T. Terlouw, T. AlSkaif, C. Bauer, W. van Sark, Optimal energy management in all-electric residential energy systems with heat and electricity storage, Appl. Energy 254 (2019), 113580, https://doi.org/10.1016/j.apenergy.2019.113580.

[30] S. Haghifam, A. Najafi-Ghalelou, K. Zare, M. Shafie-khah, A. Arefi, Stochastic bi-level coordination of active distribution network and renewable-based microgrid considering eco-friendly compressed air energy storage system and Intelligent parking Lot, J. Clean. Prod. 278 (2021), 122808, https://doi.org/10.1016/j.jclepro.2020.122808.

[31] K. Pandžić, H. Pandžić, I. Kuzle, Virtual storage plant offering strategy in the day-ahead electricity market, Int. J. Electr. Power Energy Syst. 104 (2019) 401–413, https://doi.org/10.1016/j.ijepes.2018.07.006.

[32] F. Ni, Z. Zheng, Q. Xie, X. Xiao, Y. Zong, C. Huang, Enhancing resilience of DC microgrids with model predictive control based hybrid energy storage system, Int. J. Electr. Power Energy Syst. 128 (2021), 106738, https://doi.org/10.1016/j.ijepes.2020.106738.

[33] H. Yang, Y. Zhang, Y. Ma, M. Zhou, X. Yang, Reliability evaluation of power systems in the presence of energy storage system as demand management resource, Int. J. Electr. Power Energy Syst. 110 (2019) 1–10, https://doi.org/10.1016/j.ijepes.2019.02.042.

[34] Y. Guo, Q. Wu, H. Gao, X. Chen, J. Østergaard, H. Xin, MPC-based coordinated voltage regulation for distribution networks with distributed generation and energy storage system, IEEE Trans. Sustain. Energy 10 (4) (2019) 1731–1739, https://doi.org/10.1109/TSTE.2018.2869932.

[35] O.P. Mahela, A.G. Shaik, Power quality improvement in distribution network using DSTATCOM with battery energy storage system, Int. J. Electr. Power Energy Syst. 83 (2016) 229–240, https://doi.org/10.1016/j.ijepes.2016.04.011.

[36] X. Yan, C. Gu, X. Zhang, F. Li, Robust optimization-based energy storage operation for system congestion management, IEEE Syst. J. 14 (2) (2020) 2694–2702, https://doi.org/10.1109/JSYST.2019.2932897.

[37] M. Ahmadi, O.B. Adewuyi, M.S.S. Danish, P. Mandal, A. Yona, T. Senjyu, Optimum coordination of centralized and distributed renewable power generation incorporating battery storage system into the electric distribution network, Int. J. Electr. Power Energy Syst. 125 (2021), 106458, https://doi.org/10.1016/j.ijepes.2020.106458.

[38] C. Goebel, D.S. Callaway, H. Jacobsen, The impact of state of charge management when providing regulation power with energy storage, IEEE Trans. Power Syst. 29 (3) (2014) 1433–1434, https://doi.org/10.1109/TPWRS.2013.2292434.

[39] H. Zhao, M. Hong, W. Lin, K.A. Loparo, Voltage and frequency regulation of microgrid with battery energy storage systems, IEEE Trans. Smart Grid 10 (1) (2019) 414–424, https://doi.org/10.1109/TSG.2017.2741668.

[40] N. Padmanabhan, M. Ahmed, K. Bhattacharya, Simultaneous procurement of demand response provisions in energy and spinning reserve markets, IEEE Trans. Power Syst. 33 (5) (2018) 4667–4682, https://doi.org/10.1109/TPWRS.2018.2806879.

[41] R. Khatami, K. Oikonomou, M. Parvania, Look-ahead optimal participation of compressed air energy storage in day-ahead and real-time markets, IEEE Trans. Sustain. Energy 11 (2) (2020) 682–692, https://doi.org/10.1109/TSTE.2019.2903783.

[42] G. He, Q. Chen, C. Kang, Q. Xia, Optimal offering strategy for concentrating solar power plants in joint energy, reserve and regulation markets, IEEE Trans. Sustain. Energy 7 (3) (2016) 1245–1254, https://doi.org/10.1109/TSTE.2016.2533637.

[43] A. Dahash, F. Ochs, A. Tosatto, W. Streicher, Toward efficient numerical modeling and analysis of large-scale thermal energy storage for renewable district heating, Appl. Energy 279 (2020), 115840, https://doi.org/10.1016/j.apenergy.2020.115840.

[44] Z. Parvini, A. Abbaspour, M. Fotuhi-Firuzabad, M. Moeini-Aghtaie, Operational reliability studies of power systems in the presence of energy storage systems, IEEE Trans. Power Syst. 33 (4) (2018) 3691–3700, https://doi.org/10.1109/TPWRS.2017.2771521.

[45] T. Zhao, E.A.M. Ceseña, A. Parisio, M. Panteli, J.V Milanović, Towards optimal management and control of virtual storage plants for flexible operation in future power networks, in: *Proceeding of the IEEE PES GTD Grand International Conference and Exposition Asia* (GTD Asia), 2019, pp. 583–588, https://doi.org/10.1109/GTDAsia.2019.8715913.

[46] Q. Xie, et al., Use of demand response for voltage regulation in power distribution systems with flexible resources, IET Gener. Transm. Distrib. 14 (5) (Mar. 2020) 883–892, https://doi.org/10.1049/iet-gtd.2019.1170.

[47] O.S. Nduka, et al., Field trial of coordinated control of PV and energy storage units and analysis of power quality measurements, IEEE Access 8 (2020) 1962–1974, https://doi.org/10.1109/ACCESS.2019.2961134.

[48] R.T. Elliott, et al., Sharing energy storage between transmission and distribution, IEEE Trans. Power Syst. 34 (1) (2019) 152–162, https://doi.org/10.1109/TPWRS.2018.2866420.

[49] M. Aryanezhad, Management and coordination of LTC, SVR, shunt capacitor and energy storage with high PV penetration in power distribution system for voltage regulation and power loss minimization, Int. J. Electr. Power Energy Syst. 100 (2018) 178–192, https://doi.org/10.1016/j.ijepes.2018.02.015.

[50] Y. Tan, et al., Enhanced frequency regulation using multilevel energy storage in remote area power supply systems, IEEE Trans. Power Syst. 34 (1) (2019) 163–170, https://doi.org/10.1109/TPWRS.2018.2867190.

[51] S.I. Abouzeid, Y. Guo, H.-C. Zhang, Cooperative control framework of the wind turbine generators and the compressed air energy storage system for efficient frequency regulation support, Int. J. Electr. Power Energy Syst. 130 (2021), 106844, https://doi.org/10.1016/j.ijepes.2021.106844.

[52] H. Golmohamadi, R. Keypour, Stochastic optimization for retailers with distributed wind generation considering demand response, J. Mod. Power Syst. Clean Energy 6 (4) (2018) 733–748, https://doi.org/10.1007/s40565-017-0368-y. Jul.

[53] N. Padmanabhan, M. Ahmed, K. Bhattacharya, Battery energy storage systems in energy and reserve markets, IEEE Trans. Power Syst. 35 (1) (2020) 215–226, https://doi.org/10.1109/TPWRS.2019.2936131.

[54] S. Shafiee, H. Zareipour, A.M. Knight, Considering thermodynamic characteristics of a CAES facility in self-scheduling in energy and reserve markets, IEEE Trans. Smart Grid 9 (4) (2018) 3476–3485, https://doi.org/10.1109/TSG.2016.2633280.

[55] S. Guner, A. Ozdemir, Stochastic energy storage capacity model of EV parking lots, IET Gener. Transm. Distrib. 11 (7) (May 2017) 1754–1761, https://doi.org/10.1049/iet-gtd.2016.1406.

[56] S. Guner, A. Ozdemir, G. Serbes, Impact of car arrival/departure patterns on EV parking lot energy storage capacity, in: Proceeding of the International Conference on Probabilistic Methods Applied to Power Systems (PMAPS), 2016, pp. 1–5, https://doi.org/10.1109/PMAPS.2016.7764130.

[57] A. Alahyari, M. Ehsan, M. Mousavizadeh, A hybrid storage-wind virtual power plant (VPP) participation in the electricity markets: a self-scheduling optimization considering price, renewable generation, and electric vehicles uncertainties, J. Energy Storage 25 (2019), 100812, https://doi.org/10.1016/j.est.2019.100812.

[58] U. Bin Irshad, S. Rafique, G. Town, Stochastic modeling of electric vehicle behaviour to estimate available energy storage in parking lots, IET Smart Grid 3 (6) (2020) 760–767, https://doi.org/10.1049/iet-stg.2020.0011. Dec.

[59] M.K. Daryabari, R. Keypour, H. Golmohamadi, Stochastic energy management of responsive plug-in electric vehicles characterizing parking lot aggregators, Appl. Energy 279 (2020), 115751, https://doi.org/10.1016/j.apenergy.2020.115751.

[60] M.K. Daryabari, R. Keypour, H. Golmohamadi, Robust self-scheduling of parking lot microgrids leveraging responsive electric vehicles, Appl. Energy 290 (2021), 116802, https://doi.org/10.1016/j.apenergy.2021.116802.

[61] S. Mohammad, Y. Hatim, L. Zuyi, Transmission congestion management and pricing. Market Operations in Electric Power Systems, Wiley, 2002, pp. 369–454, https://doi.org/10.1002/047122412X.ch10. Apr. 03.

[62] The Nord Pool Electricity Market, LysakerNorway. https://www.nordpoolgroup.com/.

[63] The General Algebraic Modeling Language, GAMS Software, GAMS Development Corp. and GAMS Software GmbH, 2021.

[64] The MATLAB Programming Language, The MathWorks, Inc, 2021. https://se.mathworks.com/products/matlab.html.

[65] MATPOWER The, Free, open-source tools for electric power system simulation and optimization, GitHub (2021). https://matpower.org/.

[66] H. Golmohamadi, K.G. Larsen, P.G. Jensen, I.R. Hasrat, Hierarchical flexibility potentials of residential buildings with responsive heat pumps: A case study of Denmark, J. Build. Eng. 41 (2021), 102425, https://doi.org/10.1016/j.jobe.2021.102425.

[67] Illinois Center for a Smarter Electric Grid (ICSEG), IEEE 14-bus test system, 2021, https://icseg.iti.illinois.edu/ieee-14-bus-system/.

[68] Z. Wei, Y. Li, L. Cai, Electric vehicle charging scheme for a park-and-charge system considering battery degradation costs, IEEE Trans. Intell. Veh. 3 (3) (2018) 361–373, https://doi.org/10.1109/TIV.2018.2843126.

[69] H. Farzin, M. Fotuhi-Firuzabad, M. Moeini-Aghtaie, A practical scheme to involve degradation cost of lithium-ion batteries in vehicle-to-grid applications, IEEE Trans. Sustain. Energy 7 (4) (2016) 1730–1738, https://doi.org/10.1109/TSTE.2016.2558500.